December, 18th, 2009

Technical Report on the Design and Construction of the Proton Linac of FAIR

2.7.1 System Design

2.7.1.1 The Role in the FAIR Project

A significant part of the experimental program at FAIR is dedicated to antiproton physics. For the various experiments an ultimate number of up to $7 \cdot 10^{10}$ cooled pbar/h is required. Taking into account the pbar production and cooling rate, this is equivalent to a primary beam of $2 \cdot 10^{16}$ protons/h to be provided by the chain of accelerators comprising a proton linac and the two synchrotrons SIS18 and SIS100 (Fig. 2.7.1).

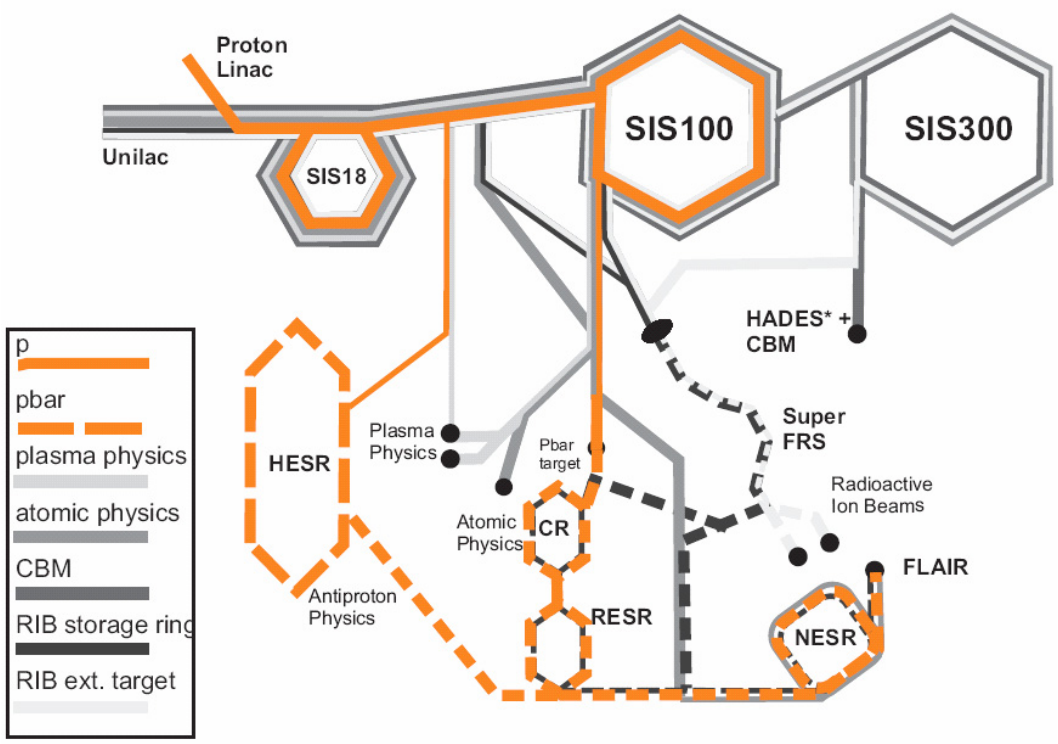

Figure 2.7.1: Schematic overview of the accelerator chain for the pbar physics program at FAIR. Proton beam lines are depicted as a solid orange line and pbar beam lines are dashed orange lines.

The achievable primary proton rate is limited by the space charge limit (SCL) in the synchrotron SIS18 being filled by horizontal multi-turn injection (MTI). During injection into the SIS100 a maximum stacking factor of 4 is achieved. Accordingly, the number of primary protons per SIS100 spill scales as the SCL of SIS18, i.e. $\beta^2\gamma^3$. The maximum rate of cooled pbars is limited by the stochastic cooling power since the cooling time scales proportional to the number of hot pbars for a sufficiently high signal-to-noise ratio. During the stochastic cooling process in the CR the SIS100 can be used to accelerate ion species different from protons.

2.7.1.2 General Description

2.7.1.2.1 Conceptual Layout

The main parameters of the linac to be fixed are its final energy and its operating frequency. Since the linac serves exclusively as injector for the synchrotron SIS18 the linac parameters can be optimized w.r.t. to the SIS18. The injection into the SIS18 is done by horizontal multi-turn injection (mti) while the SIS18 is operated at a horizontal tune of a quarter of an integer. The injected pulse current, -duration, -energy, and -emittance are coupled and at the injection a simple requirement for the injected beam brilliance is obtained as

$$B_n = 64\ \mathrm{mA/\mu m} * (\beta\gamma)^2/\eta_{mti}\ . \qquad (1)$$

B_n is the ratio of pulse current and normalized horizontal beam emittance, β and γ are the relativistic factors, and η_{mti} is the multi-turn-injection efficiency. During many years of SIS18 operation an efficiency of 60% turned out to be the best value. Accordingly, just the energy remains to be chosen, and all other beam parameters can be deduced by requiring injection up the space charge limit for protons at this energy. Higher energies provide more primary protons. In turn the linac project cost scale with the energy and energies beyond about 60 MeV suggest a jump at RF-frequency, i.e. operation at several frequencies.
The choice of 70 MeV is considered as an adequate compromise. Consequently, the required beam brilliance at the injection into the SIS follows from Equ. 1 as 17 mA/µm. The final energy of 70 MeV allows for linac operation at a single RF-frequency, i.e. 325 MHz. For that frequency fully developed rf-power sources are at hand. Secondly, the frequency is the third harmonic of the existing UNILAC Alvarez DTL. In case of its replacement by an IH/CH cavity section, the rf-equipment for 325 MHz can be used.

In order to equalize the effective number of turns at SIS18 injection for all ion species to 18, a proton current of 35 mA is required. The normalized transverse emittance of the linac follows from Equ. 1 as 2.1 mm mrad. The resulting beam pulse length is 36 µs. However, taking into account the availability of RF-power from commercial sources, the maximum design current of the linac was set to 70 mA.
The conceptual layout of the proton linac is depicted in Fig. 2.7.2, the main parameters are listed in Tab. 2.7.1. The proton beam is foreseen to be generated in an ECR type proton source and a proton current of up to 100 mA can be extracted at 95 keV. The subsequent Low Energy Beam Transport (LEBT) is based on two-solenoid magnetic focusing and provides the required separation of H_3^+, H_2^+, and H_2 fractions from the proton beam. Bunching and acceleration to 3.0 MeV will be accomplished in a 4-rod RFQ preceded by an electrostatic chopper.

Table 2.7.1: Main design beam parameters of the FAIR proton linac.

Energy	70 MeV
Maximum design current	70 mA
Current at SIS18-injection	35 mA
Protons per pulse	$7.9 \cdot 10^{12}$
Beam pulse length	36 µs (35 mA)
RF-frequency	325.224 MHz
Repetition rate	≤ 4 Hz
Beam emittance (transv., tot., norm.)	≤ 2.1 mm mrad (35 mA), 4.2 mm mrad (70 mA)
Beam momentum spread (tot., norm.)	$\leq \pm 10^{-3}$
Overall length (terminal to dump)	≈ 45 m

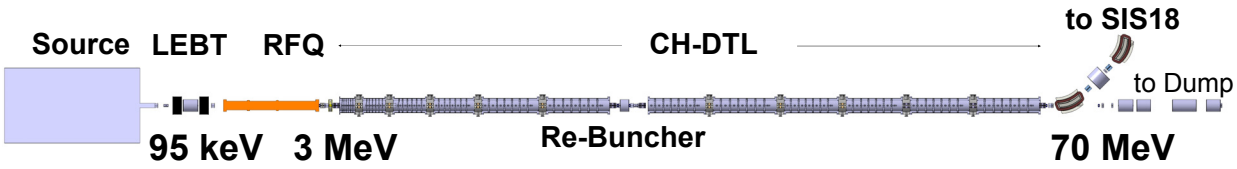

Fig.2.7.2: Conceptual layout of the FAIR proton linac comprising, a proton source, an RFQ, and a DTL based on 12 CH-cavities.

The main linac, preceded by a re-buncher for longitudinal beam matching, comprises 12 Crossed-bar H-mode cavities (CH) accelerating the beam to its final energy of 70 MeV. CH-cavities (Fig. 2.7.3) represent the extension of well established Interdigital H-cavities to higher particle velocities [1]. In connection with the applied KONUS beam dynamics [2] they provide high effective shunt impedances which in turn allow for a compact and cost efficient linac. In order to reduce the number of RF-power sources, the 12 CH-cavities are grouped to six independent pairs of RF-coupled cavities.

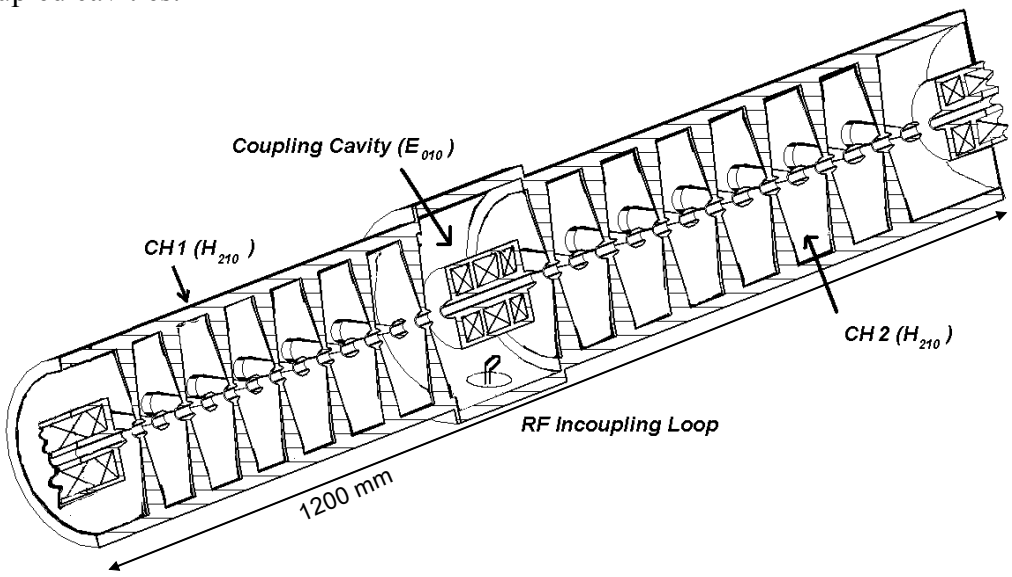

Figure 2.7.3: A pair of RF-coupled CH-cavities. The drift tubes in the centre and at the end plates will house a focusing quadrupole triplet each.

Transverse beam focusing is accomplished in quadrupole triplets housed inside the cavity end plates and in the cavity pair coupling cells. The beam dynamics layout is in progress. Full transmission of a 70 mA beam was achieved in simulations showing acceptable growth of the transverse emittances (Figs. 2.7.6, 2.7.7).]. An extended diagnostic section after the 6th CH-cavity is integrated into the DTL. It includes transverse scrapers to eliminate particles with large emittances with respect to the beam core. Additionally, a re-buncher for longitudinal re-matching into the subsequent DTL section is integrated in the section.
An advanced error analysis study was initiated [3]. Parameters that enter into beam dynamics simulations are subject to errors following a Gaussian distribution. Many runs were made with different assumptions on errors in quadrupole alignments as well as in RF-amplitudes & -phases. The sources of errors and their amount are listed in Tab. 2.7.2. A resulting beam loss scenario is plotted in Fig. 2.7.4. For time being the studies do not include corrections by steerers. This feature is currently implemented. It turned out that the losses are dominated by quadrupole translations.

Table 2.7.2: Sources and amounts of errors (rms) used for error studies.

Quadrupol translation hor., ver.	± 0.1 mm
Quadrupole rotation around hor.,ver. axis	± 1 mrad
Quadrupole rotation around beam axis	± 5 mrad
Cavity voltage error	± 1%
Single gap voltage error	± 1%
Klystron phase error	± 1°

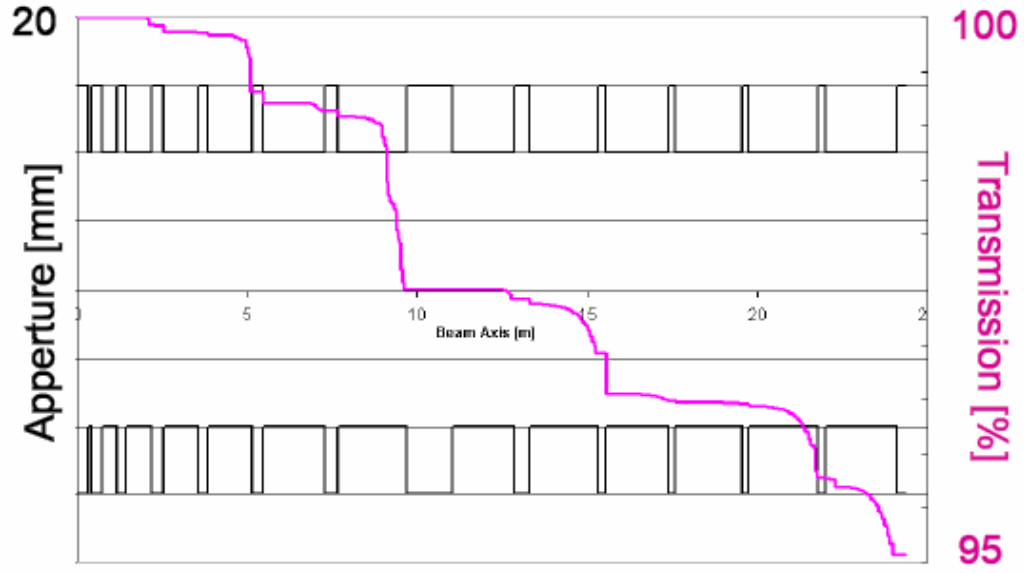

Figure 2.7.4: Uncorrected beam losses along the DTL resulting from systematic error studies on quadrupole alignment and RF-voltages and phases.

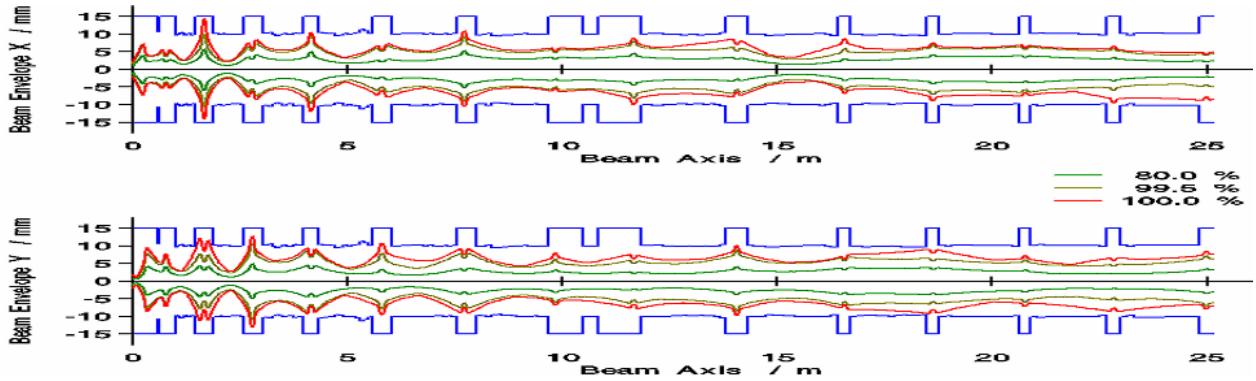

Figure 2.7.5: Simulated horizontal (upper) and vertical (lower) beam envelopes along the DTL section for a current of 70 mA.

The RF-pulse length of 200 µs (Chap. 2.7.4) and a maximum repetition rate of 4 Hz result in a low RF-duty factor of 0.08%. This simplifies the mechanical design of the normal conducting RF-cavities with respect to cooling.
After an achromatic 90°-inflection into the existing transfer channel UNILAC-SIS18, a third re-buncher tilts the longitudinal phase space distribution in order to provide a minimized momentum spread at injection into the synchrotron SIS18.

Within the design of the full linac end-to-end beam dynamics simulations were performed. They start from a thermal distribution in the ion source plasma chamber and they end at the injection septum of the synchrotron SIS18. Six codes have been used:

source extraction:	AXE-INP
to RFQ-input:	SOLMAX and TraceWin
to RFQ-exit:	DYNAMION
to DTL-exit:	LORASR
to synchrotron:	PARMILA Transport

AXE-INP is a 2d-PIC code. SOLMAX calculates the time and space dependence of the space charge compensation based on Monte-Carlo interaction of the residual gas with the beam. It is used in an iterative scheme together with TraceWin being a 3d-PIC code for particle tracking. DYNAMION is a 3d-particle-particle code. Since it is more pessimistic than other RFQ codes it has been used. Additionally, it was benchmarked successfully with several measurements at the UNILAC RFQ and DTL. LORASR is a 3d-PIC code and PARMILA is a transport code using the SCHEFF routine for space charge handling.

In order to fill the SIS synchrotron up to its space charge limit with protons at 70 MeV, the horizontal normalized beam brilliance, i.e. pulse current per normalized total emittance, must not be less than 17 mA/mm mrad. This means in turn that the normalized emittance per current must be less than 0.06 mm mrad/mA. In order to judge whether a given distribution is suited for injection, it should be analyzed with respect to its brilliance: the fractional emittance is plotted as a function of the number of particles (current) used for the emittance evaluation. Within the same graph the straight line corresponding to 0.06 mm mrad/mA is plotted. We have created these graphs at the exit of several sections along the beam line and they are shown in chapters

corresponding to these sections. Figure 2.7.6 plots the graph at the injection into the SIS18. It shows that the horizontal brilliance requirement is met up to a current of about 76 mA and for all currents below that value. Additionally, for the design current of 70 mA the corresponding horizontal emittance was evaluated that contains this current. This evaluation was made at the exit of several section of the linac beam line. The result is shown in Fig. 2.7.7 demonstrating that the final beam current is within 3.0 mm mrad being well below the design value of 4.1 mm mrad.

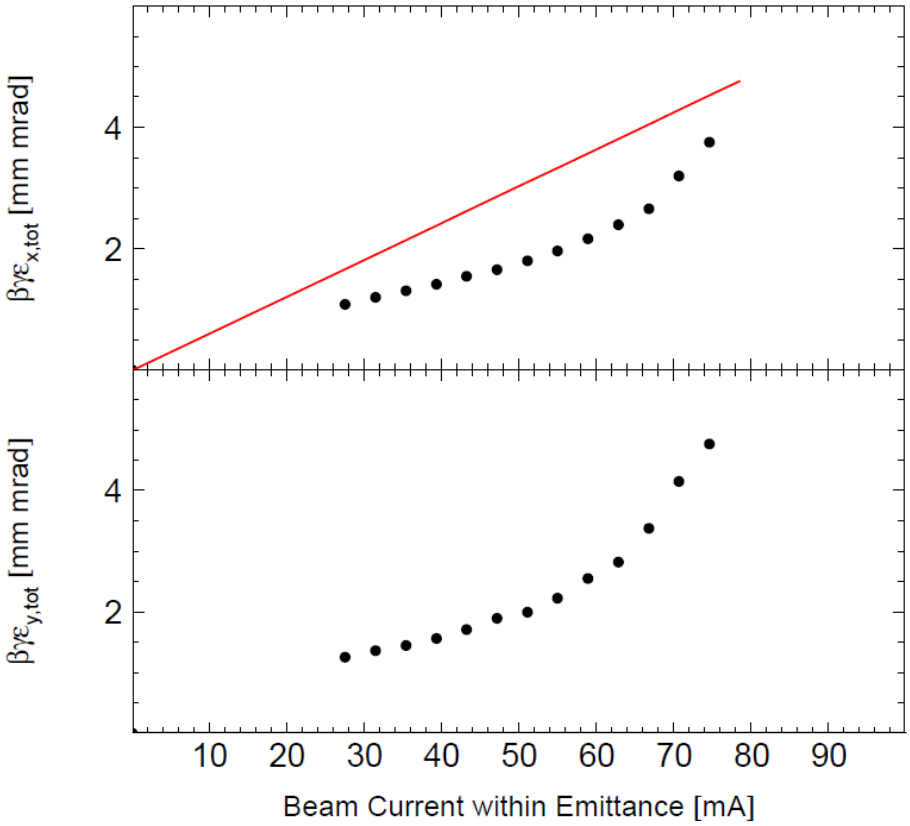

Figure 2.7.6: Normalized total emittance as function of the beam current confined by the emittance at the injection to the SIS18. The required brilliance at the SIS18 is indicated by a red line.

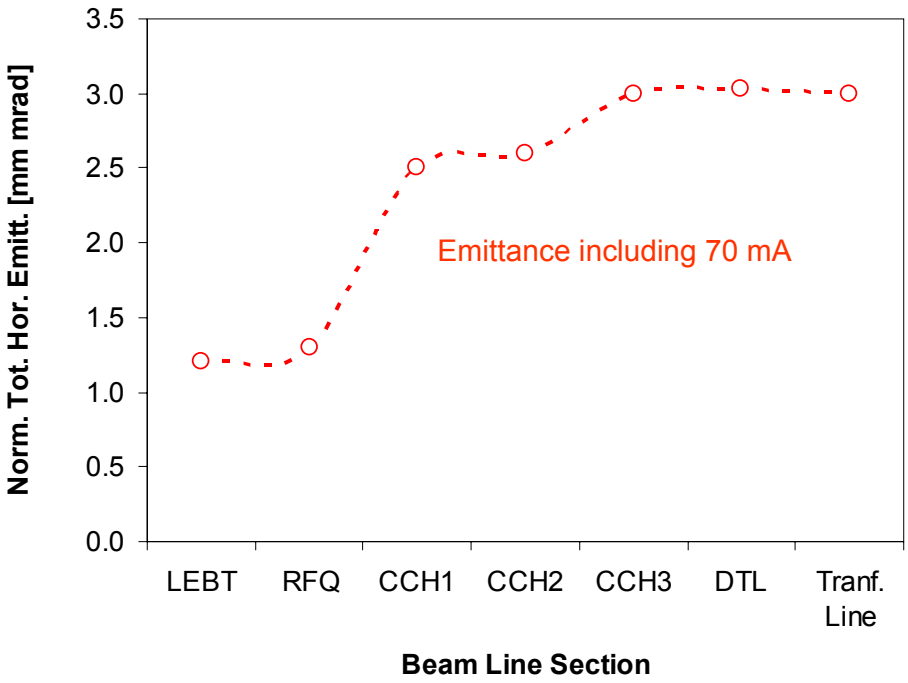

Figure 2.7.7: Normalized total horizontal emittance containing 70 mA at the exit of several beam line sections of the linac beam line.

The strongest emittance growth occurs after the RFQ due to the change of beam aperture. Non-adiabatic change of beam dimensions along the MEBT section causes mismatch which in turn drives emittance growth. At the injection into the synchrotron also the longitudinal acceptance criteria of the synchrotron must be met. A final re-buncher in the transfer line provides for minimized momentum spread. Figure 2.7.8 shows the particle distribution as obtained from end-to-end simulations at the injection into the SIS, demonstrating that the full current is within the longitudinal acceptance of ±0.1% of relative momentum deviation.

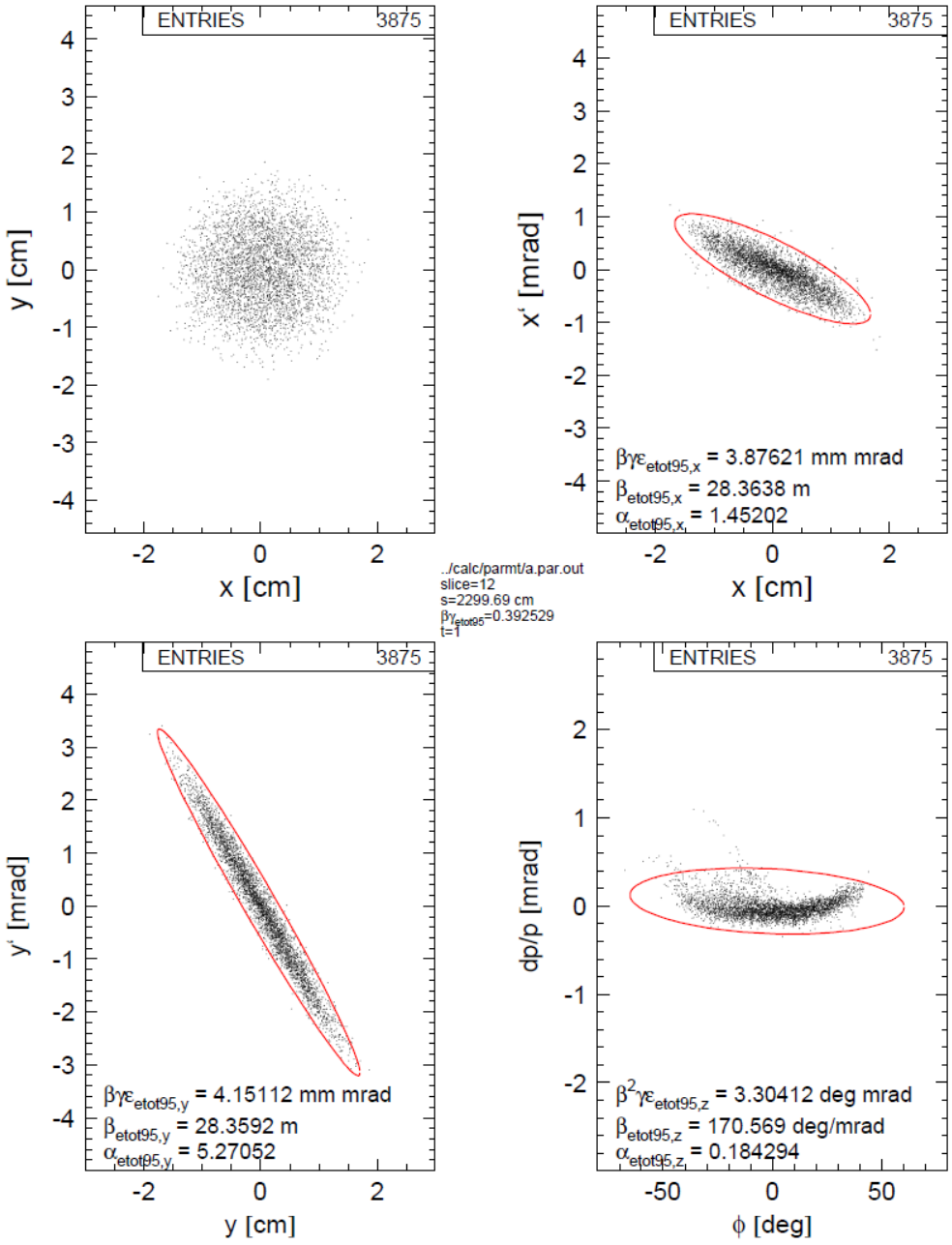

Fig. 2.7.8: Distribution at the injection into the synchrotron SIS18 as obtained from end-to-end simulations.

2.7.1.2.2 System Parameters

The basic beam parameters and technical parameters of the proton linac are summarized in Tab. 2.7.3.

Table 2.7.3: Main design parameters of the FAIR proton linac.

Proton Source	
source type	ECR
beam pulse length	500 µs
proton fraction	≥ 70%
extracted proton current	≥ 100 mA
extraction voltage	95 kV
LEBT	
focusing scheme	2 solenoids
molecule fraction analysis (H^+, H_2^+, H_3^+)	Allison scanner
beam chopping	electrostatic
output proton current	100 mA
output emittance (norm., tot.)	≤ 1.8 mm mrad
mechanical length incl. Chopper	≤ 2.16 m
RFQ	
cavity type	4-rod, water cooled
output energy	3.0 MeV
cavity cooling requirements	water, 10 l/min, T_{out}–T_{in} ≤ 4 K, δT ≤ ± 2 K
max. accelerated output current	≥ 90 mA
output emittance (transv., norm., tot.)	≤ 2.0 mm mrad
output emittance (long., tot)	≤ 930 keV deg
cavity Q_0-value	2500 - 8000
total RF-power (peak)	≤ 1.0 MW
electric field strength	≤ 36.6 MV/m = 2.0 E_k
mean aperture radius	≤ 3.9 mm
mechanical length	≤ 3.5 m
Drift Tube Linac	
number of RF-cavities	12, grouped to 6 independent pairs
cavity type	Crossed-bar H-cavity (CH), water cooled
cavity cooling requirements	water, 10 l/min, T_{out}–T_{in} ≤ 4 K, δT ≤ ± 2 K
output energy	70 MeV
maximum design output current	70 mA (within design emittance)
current at injection into SIS18	35 mA (within design emittance)
output emittance (transv., norm., tot.)	≤ 2.1 mm mrad (35 mA), 4.2 mm mrad (70 mA)
output momentum spread Δp/p (tot.)	≤ $\pm 10^{-3}$ (at SIS18 injection)
cavity Q_0-value	16500 – 18000
single tank length	0.40 – 2.00 m
number of gaps per cavity	9 – 15
tot. RF-power per pair of cavities (peak)	≤ 2.5 MW
accelerating field strength	8.5 – 2.8 MV/m (depending on part. velocity)
ratio $E_{surface}$ / E_{acc}	≤ 4.3, i.e. $E_{surface}$ ≤ 1.9 E_k
effective shunt impedance	93 – 41 MΩ/m (depending on part. velocity)
focusing scheme (transv.)	separated function quadrupole triplets
focusing scheme (long.)	KONUS [2]
mechanical length	≈ 24 m
Beam Pulse Time Structure	
RF-frequency	325.224 MHz
RF-pulse length	200 µs
beam pulse length	≤ 36 µs
repetition rate	≤ 4 Hz

2.7.2 Magnets

All magnets for the proton linac are operated at room temperature. Their position along the beam line is shown in Fig. 2.7.9 and their main design parameters are listed in Tab. 2.7.4.

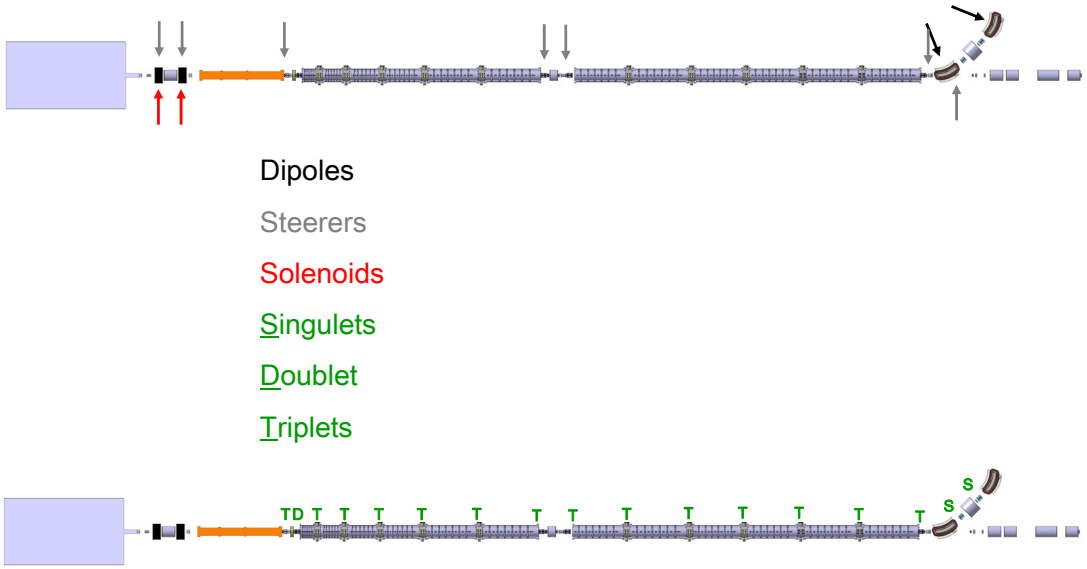

Fig. 2.7.9: Position of the magnets along the linac beam line.

Although the main purpose of the linac is to deliver protons to generate antiprotons for the physics program, the accelerator chain might occasionally request proton beams at reduced proton intensities for dedicated experiments. Due to the high space charge forces in the linac, different beam optics need to be applied for different beam currents. Additionally, to reduce operation cost all magnets (but the LEBT solenoids and steerers) and their power converters are designed for pulsed operation.

Table 2.7.4: Main design parameters of the proton linac magnets, i.e. type, location, number to be used, field strength or field gradient, effective field length, and aperture radius.

Type	Location	#	B(B') / T(T/m)	Leff. /mm	Ap. Rad./mm
Solenoid	LEBT	2	0.7	267	125
Steerer (hor/ver)	LEBT	2	B*L_eff = 0.0012 Tm		125
Steerer (hor/ver)	DTL	4	B*L_eff = 0.0125 Tm		15
Steerer (hor/ver)	Dump	1	B*L_eff = 0.0125 Tm		33
Quad Type C	MEBT, DTL	14	67	90	15
Quad Type D	DTL	30	67	50	15
Quad Type E	Inflect., Dump	2	40	179	20
Dipole 45°	Inflection	2	1.30	785.3	20*20 (hor*ver)

2.7.2.1 Solenoids

Two solenoids will be used in the LEBT section. Each solenoid will be powered individually. Their layout is taken from the solenoids for the IFMIF project [4] as shown in Fig. 2.7.10. The solenoids for IFMIF are under production. The minor adoptions of the design to meet the general FAIR standards are currently integrated such that the delivery of the solenoids for the FAIR proton linac solenoids is expected in late 2010.

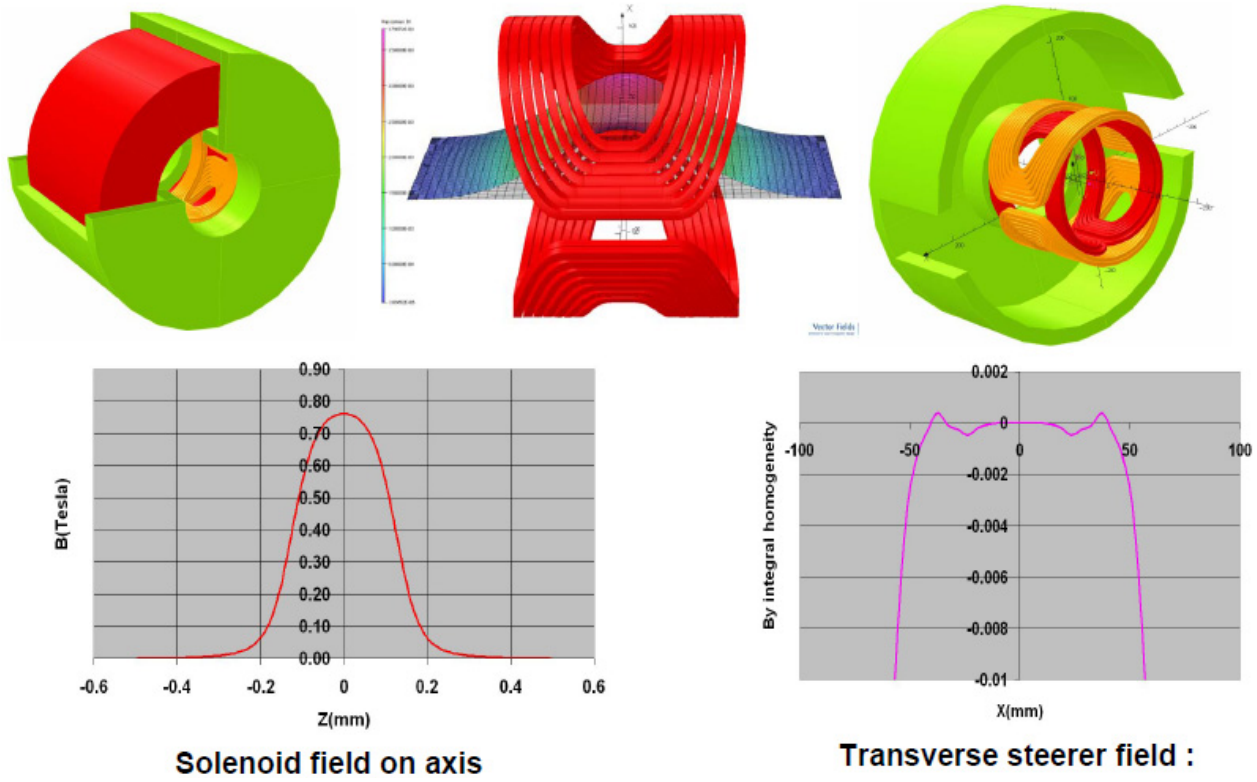

Fig. 2.7.10: Conceptual layout of the IFMIF solenoids with integrated steerers [4].

2.7.2.2 Steering Magnets

In total seven steerer pairs (horizontal/vertical) are foreseen to be installed in the linac, each of them powered individually. Two steerers in the LEBT allow for on-axis injection into the RFQ; one steerer directly behind the RFQ corrects eventual angle offsets at the RFQ exit; along the DTL section three steerers are foreseen: two within the extended drift between the 6th and the 7th CH-cavity, one after the last cavity, and a last one at the beam line towards the dump.

2.7.2.3 Quadrupole Magnets

Three different types of quadrupole lenses are used along the linac and the beam transport sections. Along the DTL triplets are used made of quadrupole types C-D-C, with a prolonged lens in the centre. All quadrupoles used along the DTL have the same aperture. Outer quadrupoles of triplets are powered in series except for the triplet after the RFQ and the triplet after the last cavity of the DTL.

The two singulets (quadrupole type E) along the achromatic inflection into the existing transfer channel are powered in series. Their aperture is increases by 33% w.r.t. to the DTL quadrupoles. Figs. 2.7.11 and 2.7.12 show the conceptual layout of the quadrupoles.

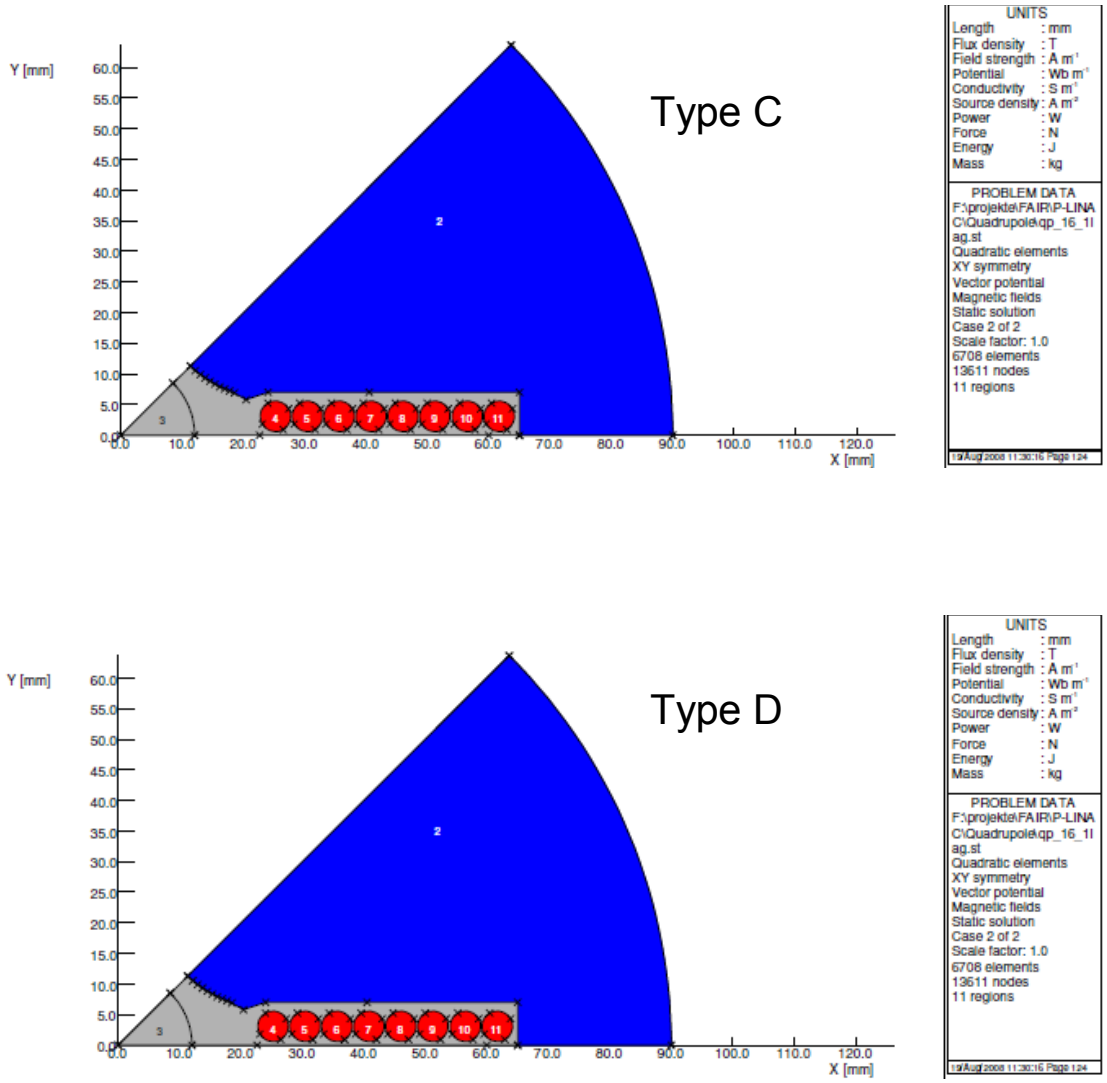

Fig. 2.7.11: Conceptual layout of quadrupole type C (upper) and D (lower) used in the DTL.

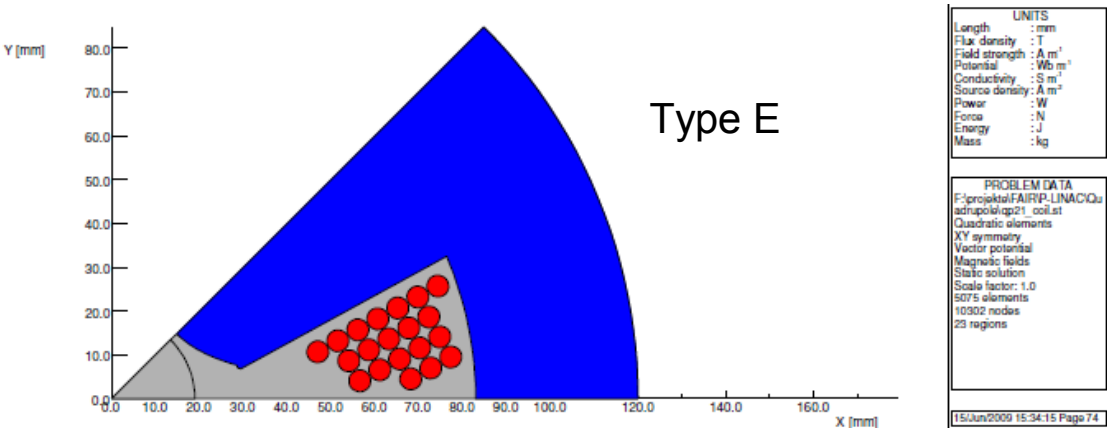

Fig. 2.7.12: Conceptual layout of the dipole used in the inflection.

2.7.2.4 Dipole Magnets

The two inflection dipoles deflect the beam twice by 45° into the transfer channel UNILAC-SIS18. In case of intolerable beam losses the dipoles are set to zero deflection in order to dump the beam in forward direction. For this purpose each dipole will be equipped with a Hall probe. The dipoles have the same horizontal and vertical aperture. To assure proper zero-field control, each dipole is powered individually. Figure 2.7.13 shows their conceptual layout.

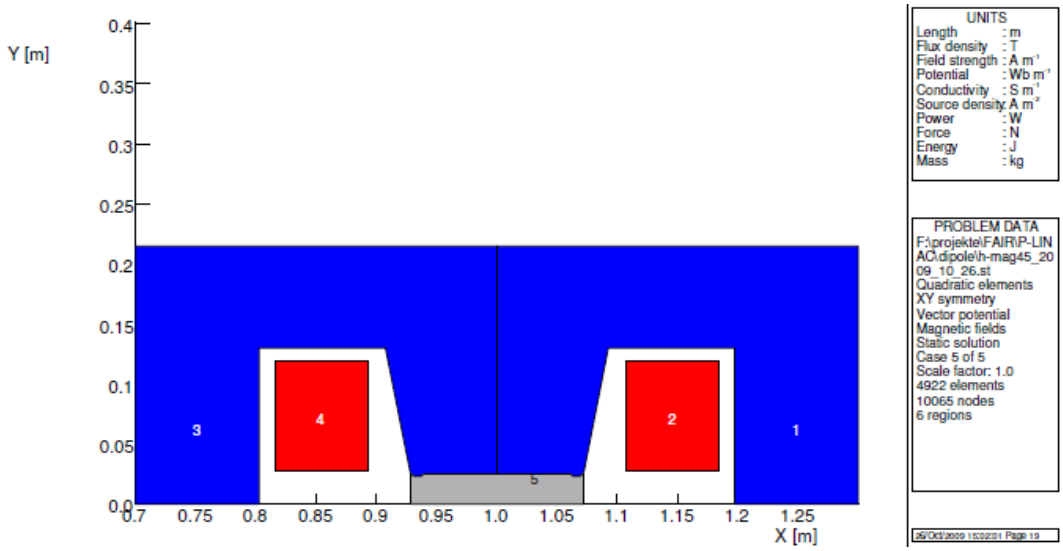

Fig. 2.7.13: Conceptual layout of quadrupole type E used in the inflection.

2.7.3 Power Converters

The main parameters of the proton linac power converters are listed in Tab. 2.7.5. For details we refer to the subsequent subchapters.

Table 2.7.5: Main parameters of the proton linac power converters, i.e. type, number to be used, load, maximum current, maximum voltage, maximum power, apparent power, and rise time. Parameters not been defined yet are indicated as "tbd".

Type	#	Load	Imax/A	Umax/V	Pmax/kW	Papp/kW	T/ms
Magnets							
Solenoid	2	Solenoid	415	42.0	17.6	18.8	dc
PS_S1	4	Steerer_S1	200	7.1	1.4	1.7	25
PS_S2	10	Steerer_S2	200	7.1	1.4	1.6	25
PS_QA	14	Quad_C	946	45.4	42.9	5.4	25
PS_QA	8	Quad_D	963	39.8	38.3	5.2	25
PS_QB	11	Quad_D – Quad_D	963	67.5	65.0	7.6	25
PS_QC	1	Quad_E – Quad_E	369	102	37.5	3.5	25
D1	2	Dip_45°	905	569	515	13.5	25
RF-pow.							
Kl_HV	7	Klystron Cathode	60	-1.10E05	tbd	tbd	0.2
Kl_An	7	Klystron Anode	0.02	-1.13E5	tbd	tbd	0.2
Kl_Heat	7	Klystron Heater	30	15	0.45	0.45	dc
Kl_Sol_1	7	Klystron Sol_1	20	20	0.4	0.4	dc
Kl_Sol_1	7	Klystron Sol_2	20	375	7.5	7.5	dc
Kl_Sol_2	7	Klystron Sol_3	20	94	1.88	1.88	dc

2.7.3.1-4 Magnet Power Converters

The design of the magnet power converters is straight forward. The load data are based on the magnet design specifications and on the supply cable lengths. Cost and sizes of the power converters are estimated with high reliability. The power converters of the steerers and of the quadrupoles are designed very compact, such that two independent power converters fit into one standard rack of 800 mm width.

2.7.3.5 RF-Power Source Power Converters

The RF-power sources together with their power converters represent a considerable part of the overall project cost. In order to obtain an optimized concept, different scenarios of the RF-power alimentation for the given number of RF-cavities were investigated technically and with respect to investment cost. Nine different scenarios based on different RF-power source types and on different circuit options (No. of cavities per RF-source, No. of RF-sources per power converter) were studied in detail and their costs were estimated based on vendor quotations [5]. It was found that a solution based on one power converter driving one klystron which in turn drives one RF-coupled pair of cavities results in the best price.

The power converters for pulsed klystrons at 325 MHz need special efforts for the design, specification, and production. Converters for cw-klystrons were operated at LEP. However, for a pulsed machine at this frequency converters are not available yet. For the FAIR proton linac the development aims for devices that can be operated without crow bars in order to be efficient in cost and spacing. The specifications of the oil-free set-up are available and the call for tender for the first device has been launched in November 2009. Delivery is expected in early 2011.

One power converter system driving a klystron comprises six power converters as shown in Fig. 2.7.14. The main converter (PS1) has to deliver the klystron electron beam current pulse of 60 A with a cathode-to-ground voltage of 110 kV. It delivers pulses of 200 µs at 4 Hz. Assuming an electron current of 60 A, a total charge of about 12 mC is required per RF-pulse. This charge is stored in a capacitor of 1 µF such that the total amount of energy that might be released in case of a voltage break down (arc voltage of 100 V) will not exceed 11 J (100 V · 110 kV · 1 µF), which is not critical for the klystron. The main part of the energy released in case of a break down, i.e. the equivalent to the total charge in the 1 µF capacitor, will be dissipated in a resistor of about 30 Ω being in series with the klystron cathode. During the pulse the voltage droop at the capacitor needs to be compensated such that the total droop does not exceed 0.5%. In the time between pulses the capacitor is re-charged by a 110 kV / 20 mA high voltage source. The pulse rise/fall time is 10 µs at maximum.

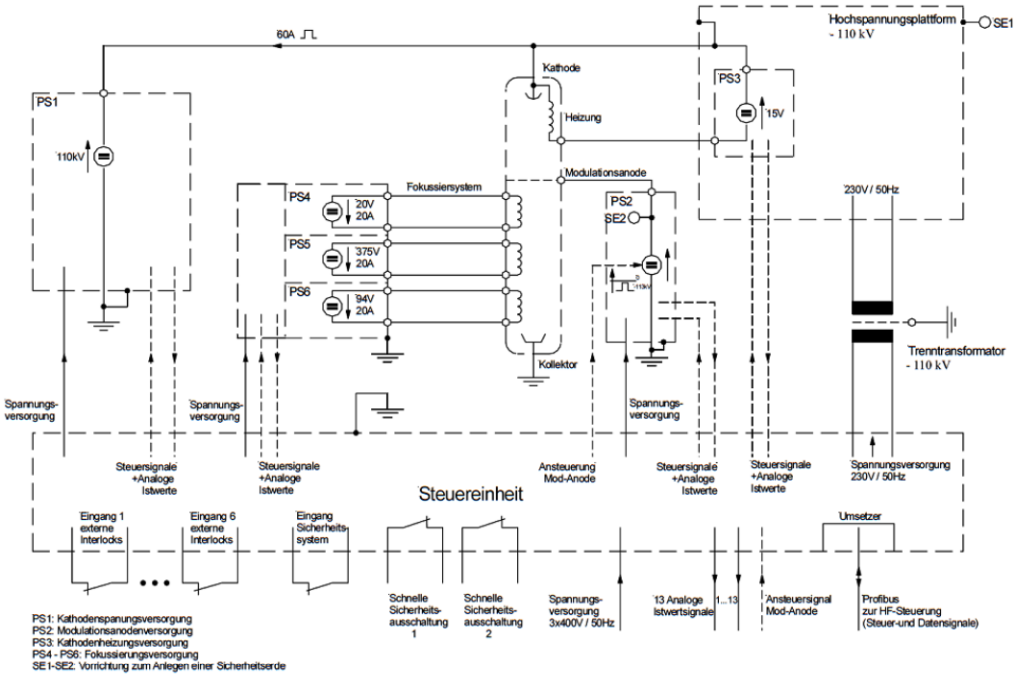

Fig. 2.7.14: Conceptual circuit diagram of the klystron power converter.

A second converter (PS2) provides the voltage of the modulation anode to control the electron beam current. The modulation anode can be completely opened by applying 0 V. Between pulses up to -113 kV can be applied, i.e. -3 kV w.r.t. the anode, in order to gate the anode. The fall/rise time of the modulation anode voltage is less then 5 µs. Finally, a dc cathode heater power converter (PS3) as well as dc-converters for the solenoid circuits (PS4-PS6) is required.

2.7.4 RF-Systems

2.7.4.1 RF-Power Sources

For a pair of RF-coupled CH-cavities the total amount of required peak RF-power including safety margin is 2.5 MW at maximum. As pointed out in Chap. 2.7.3.5 ten different RF-power alimentation schemes employing different RF-power sources were investigated in detail [5]. The three re-bunchers require RF-sources with an output power of less then 50 kW, implying the use of tube amplifiers with integrated power converters as already operated at GSI.

2.7.4.1.2 Klystrons

The RF-pulse to be provided by the power sources for each pair of cavities is shown in Fig. 2.7.15. During the beam pulse, the total forward RF-power is 2.5 MW at maximum and about half of this value for the unloaded cavities. The stability must be better than 0.1%.

A survey on the market with respect to available power sources indicated that adapting the Toshiba klystron 3740A® gives a minimum in investment cost. This klystron is designed for an operation frequency of 324 MHz, a routine operation output peak power of 2.5 MW, and a duty cycle of 3.25%. It is employed at the JPARC linac and it will be used at the ISIS project. Adapting to our frequency of 325.224 MHz was straight forward. Seven klystrons will be used in total, i.e. six to power the DTL cavities and one for the RFQ. The rf-bandwidth is ± 0.75 MHz. The first Toshiba klystron has been delivered to GSI in April 2008 (Fig. 2.7.16).

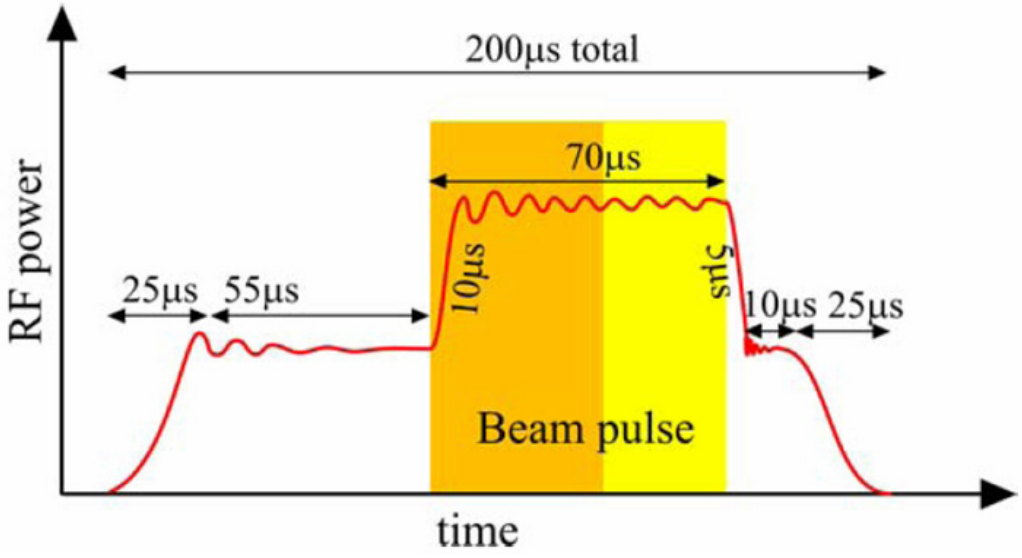

Figure 2.7.15: Shape of the RF-pulse to be provided by the RF-power sources for the accelerating cavities of the proton linac including a safety margin of 25%. The RF-power is initially switched on and regulated to the unloaded cavity level. The input power is increased within less than 10 ns after the beam entered into a pair of two RF-coupled cavities.

The high RF-power sources of the linac comprise a major part of the space requirements for the building of the linac complex. Two levels are used to house the different components related to RF as shown in Fig. 2.7.17. The klystron power converters are installed at ground level while the klystrons are lifted to the second floor. Waveguides feeding the RF into the cavities couple the power to the cavities from top. To this end a dedicated intermediate floor is integrated just above the linac tunnel. This floor will house also the circulators and loads for reflected power.

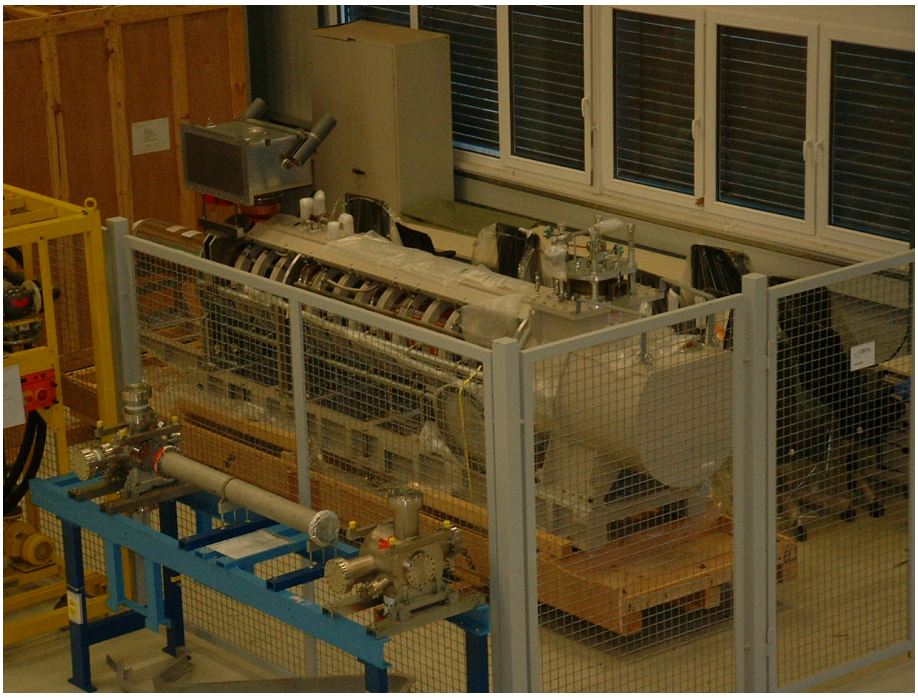

Figure 2.7.16: A modified version of the Toshiba klystron 3740A® used at J-PARC has been delivered to GSI in April 2008.

2.7.4.1.6 Tube Amplifiers

The three re-bunchers need RF-power of less than 50 kW and solutions based on conventional tube amplifiers as already used at GSI are foreseen. However, klystron manufacturers were contacted as well in order to receive proposals.

2.7.4.1.10 Timing, Tuning, Local Controls

The low-level system is currently under construction and will be fully tested after delivery of the klystron power converter in early 2011. The main control unit of one RF-power source is a SPS unit. All parameters to be received and to be send by the unit have been defined as well as the corresponding protocols. Required interlocks and fast switch-off procedures have been defined of which a major part has been provided by the klystron manufacturer. Figure 2.7.18 depicts the signal circuit of the RF-controls.

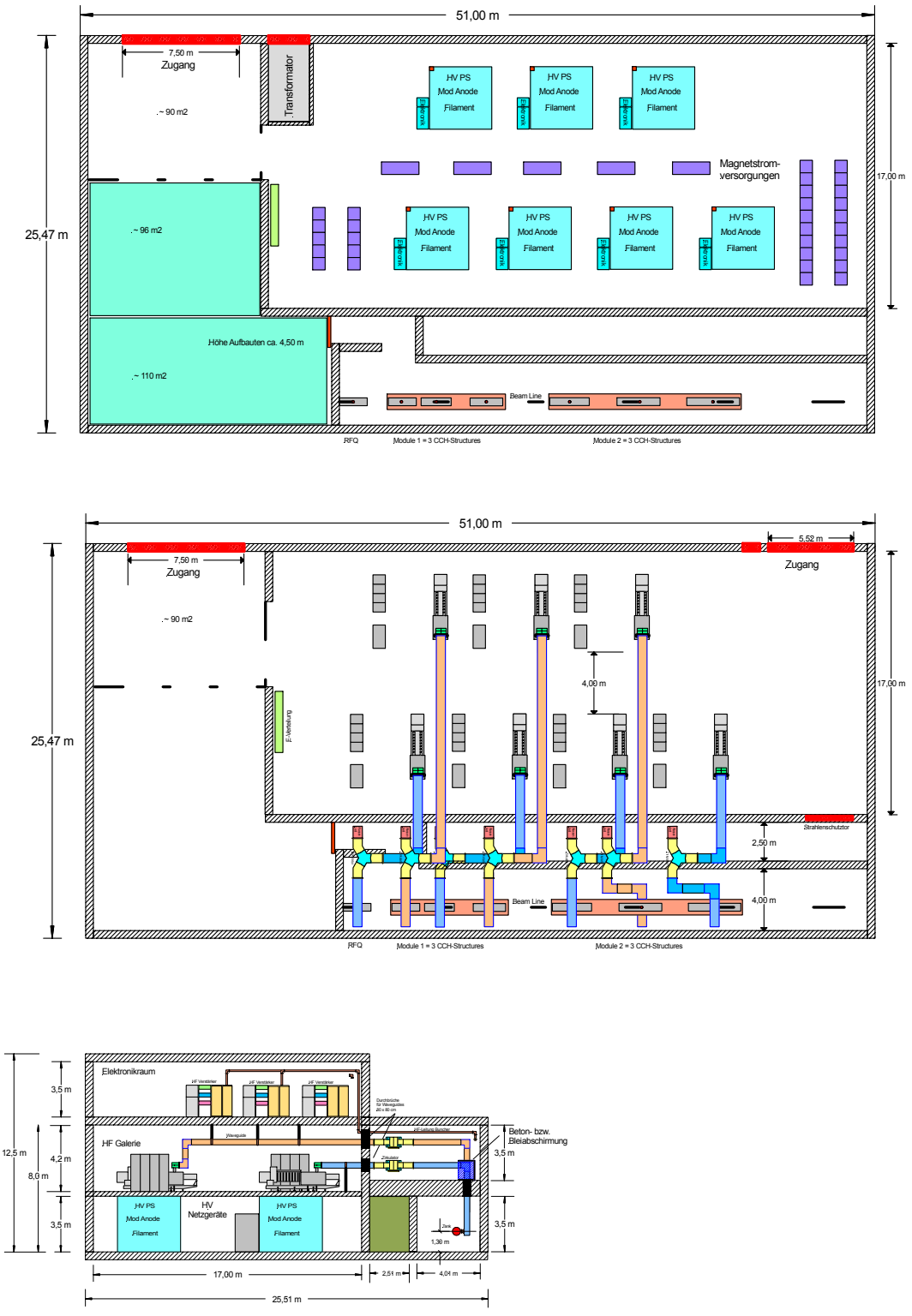

Fig. 2.7.17: RF-installations in the proton linac building complex. Upper: top view ground floor; centre: top view first floord; lower: view from West.

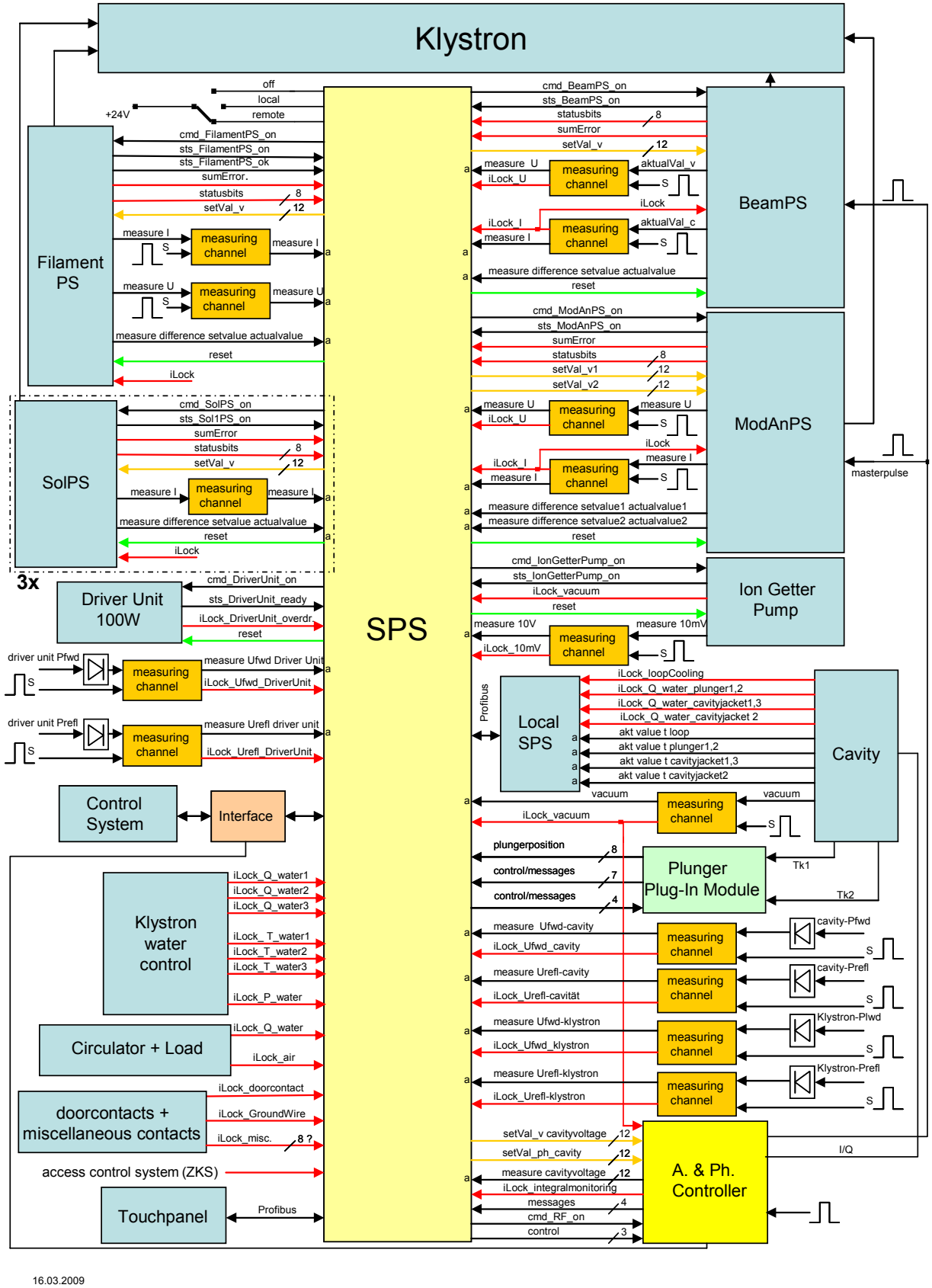

Fig. 2.7.18: Signal circuit of the RF-controls for the proton linac.

2.7.4.2 RFQ Cavity

The beam parameters at the entrance to and at the exit of the RFQ were defined and are listed in Tab. 2.7.3. At frequencies above 300 MHz cavities of the 4-vane type are commonly in use as for example the LEDA-, IPHI-, and the BARC-RFQ [6,7]. The investment cost for these RFQs are usually significant. This is partially due to the high duty cycles of the respective machines and to the corresponding cooling efforts. As an alternative, a 4-rod type RFQ is much simpler in mechanical design and thus less expensive. However, it has not been built so far for frequencies above 300 MHz. The University of Frankfurt gained huge experience on 4-rod RFQs and a conceptual design for the RFQ of the FAIR proton linac is available [8].

The design uses the novel so-called New Four-Section Procedure (NFSP) [9]. This procedure abandons the common rule of constant transverse focusing along the whole structure. Figure 2.7.19 plots the various RFQ parameters, i.e. synchronous phase & energy, aperture, and voltage as a function of the RFQ cell number.

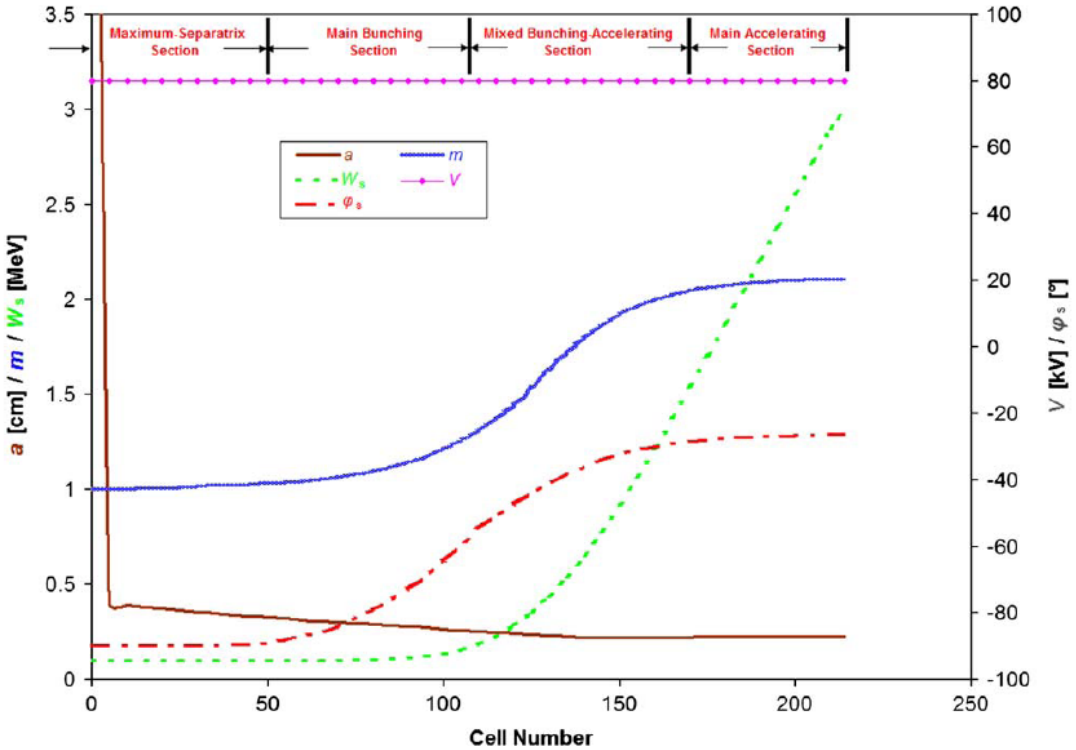

Fig. 2.7.19: RFQ parameters as a function of the cell number, i.e. synchronous phase & energy, aperture, and voltage.

In the first section serves exclusively for beam bunching and does not accelerate. Accordingly, the synchronous phase is constant at -90°. The modulation starts very smoothly. Along the following section the transverse focusing is increased to compensate for the increased transverse defocusing of the bunched beam. The phase moves towards higher values to provide acceleration. After reaching sufficient velocity at the entrance to the third section, the transverse focusing can be reduced again, thus reducing also the longitudinal emittance growth. The final section provides acceleration up to the final energy. Synchronous phase and modulation are kept constant.

With a maximum surface electric field of less than two Kilpatrick (E_k) a transmission of accelerated particles of 98% is reached using the PARMTEQ simulation code. Low energy

particles which are not trapped into RF-buckets comprise less than 1% of the overall intensity. The normalized transverse emittance of 1.5 mm mrad is well below the design value of 2.0 mm mrad. For the design of the RFQ the code PARMTEQM has been used. The design aimed for a wide bandwidth w.r.t. the input current. To this end the RFQ was designed for 45 mA of input current using the PARMTQM code. Afterwards the robustness of the design has been checked by varying the input current up to 100 mA. The input emittance as well as the RFQ voltage has been kept constant. Figure 2.7.20 shows the transmission as a function of the cell number for three different currents, i.e. 45 mA, 70 mA, and 100 mA. For the higher currents two cases have been investigated: (1) the beam matching at the entrance has been set as for the 45 mA case. (2) The matching has been adopted to the higher current. It was demonstrated that even for 100 mA 98% of transmission can be reached without re-adjustment of the matching at the RFQ entrance.

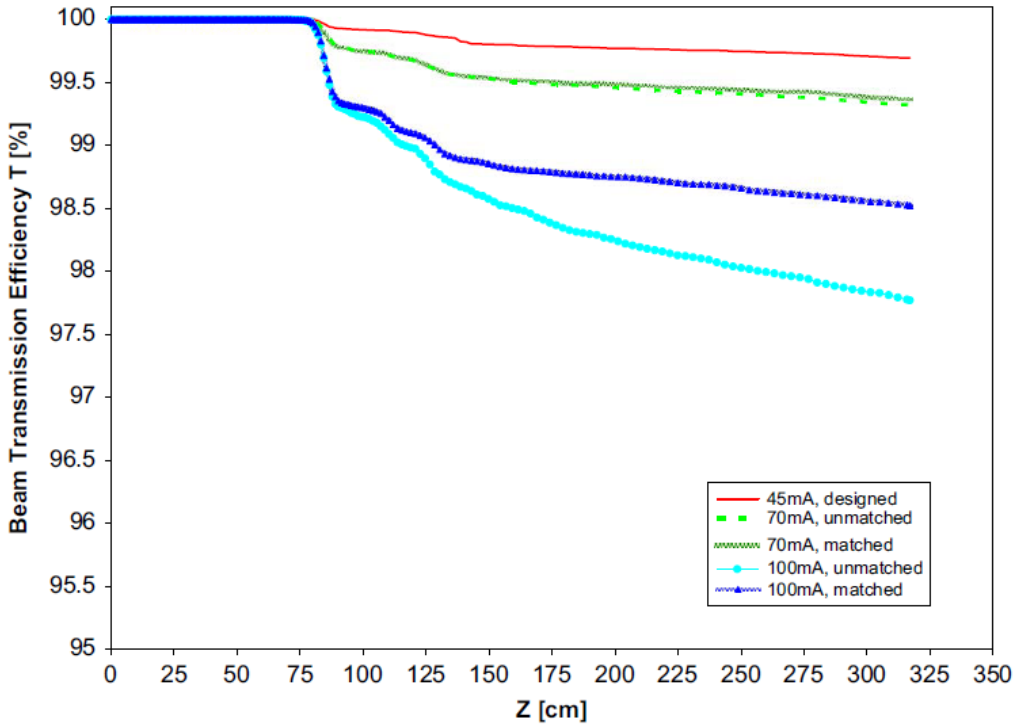

Fig. 2.7.20: RFQ transmission as a function of the cell number for different input currents and matching settings at the RFQ entrance. The PARMTEQM code was used for this study.

For the RFQ design current of 45 mA the applied simulation code, i.e. PARMTEQM, has been benchmarked with DYNAMION [10] and TOUTATIS [11]. Starting from a 4d-Waterbag distribution at the RFQ entrance, the final emittances and transmissions at the RFQ exit have been compared and are listed in Tab. 2.7.6.

Tab. 2.7.6: Comparison of final beam parameters for three simulation codes.

	PARMTEQM	TOUTATIS	DYNAMION
Transmission [%]	99	99	94
hor. rms-emittance (norm.) [mm mrad]	0.30	0.30	0.35
ver. rms-emittance (norm.) [mm mrad]	0.30	0.30	0.36
long. rms-emittance [MeV deg]	0.16	0.16	0.16

The code benchmarking revealed very similar results from PARMTEQM and TOUTATIS, while DYNAMION delivered lower transmission and stronger emittance growth. For this reason the further beam dynamic investigations have been done using the DYNAMION code.
Although not finally decided, the most likely operation of the linac front end will be an injection current into the RFQ of 80 mA. The full current of 100 mA will be extracted from the source and an iris between the two LEBT solenoids will remove the outer 20% of the current. Therefore the parameter studies of the RFQ were done using a current of 80 mA. For details of the study we refer to the dedicated report [12].
The particle transmission has been simulated keeping the current constant and varying the input emittance and vice versa. As input distribution a Gaussian truncated at 2σ was assumed. Figure 2.7.21 plots the transmission of accelerated particles as a function of the input current being varied from 0 to 120 mA. The total input emittance was kept constant at 1.5 mm mrad. At very low currents 100% transmission is achieved. However, at 80 mA it drops to 91%.

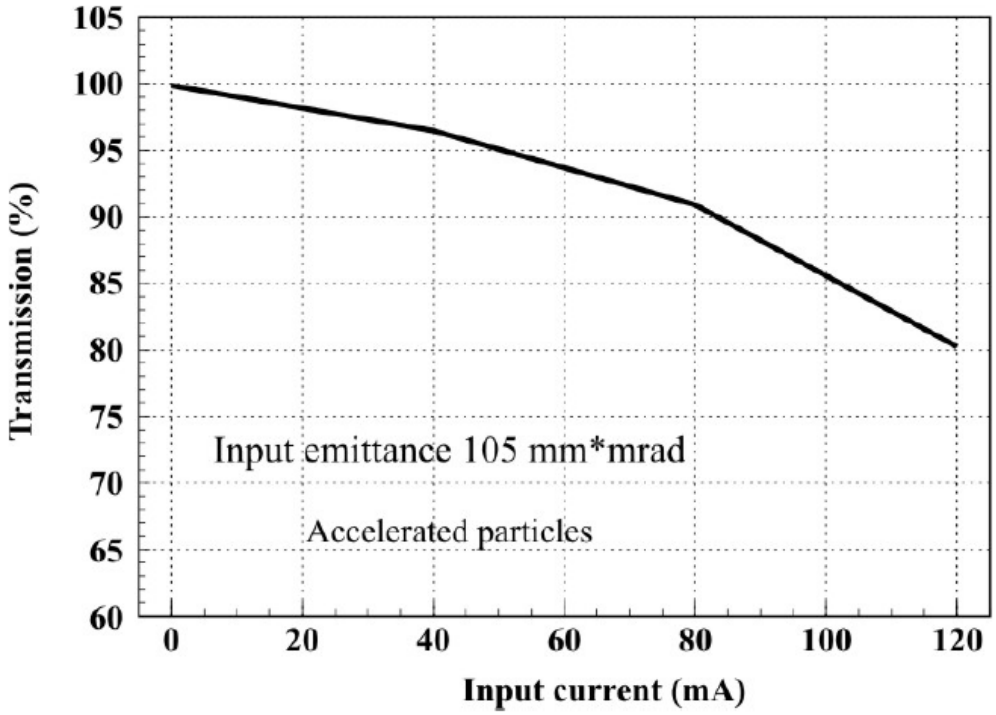

Fig. 2.7.21: RFQ transmission as a function of the input current for a constant total input emittance as simulated using the DYNAMION code.

Figure 2.7.22 shows the complementary scan, i.e. the transmission of accelerated particles as a function of the input emittance for a constant current of 80 mA. Increasing the input emittance from 1.5 mm mrad to 3.7 mm mrad (norm.) leads to a drop of transmission from 92% to about 50%.
Parameters studies generally assume artificial distributions from text books. However, real distributions most likely will be different. In order to address this issue as input a result from a preceding beam dynamics simulation of the source/LEBT set-up has been used. This distribution is shown in Fig. 2.7.47. Its shows a manifold of filamentations and it is obviously different from any distribution to be described analytically. It even exhibits a finit longitudinal emittance, i.e. a non-zero initial energy spread, being generally neglected in RFQ design.

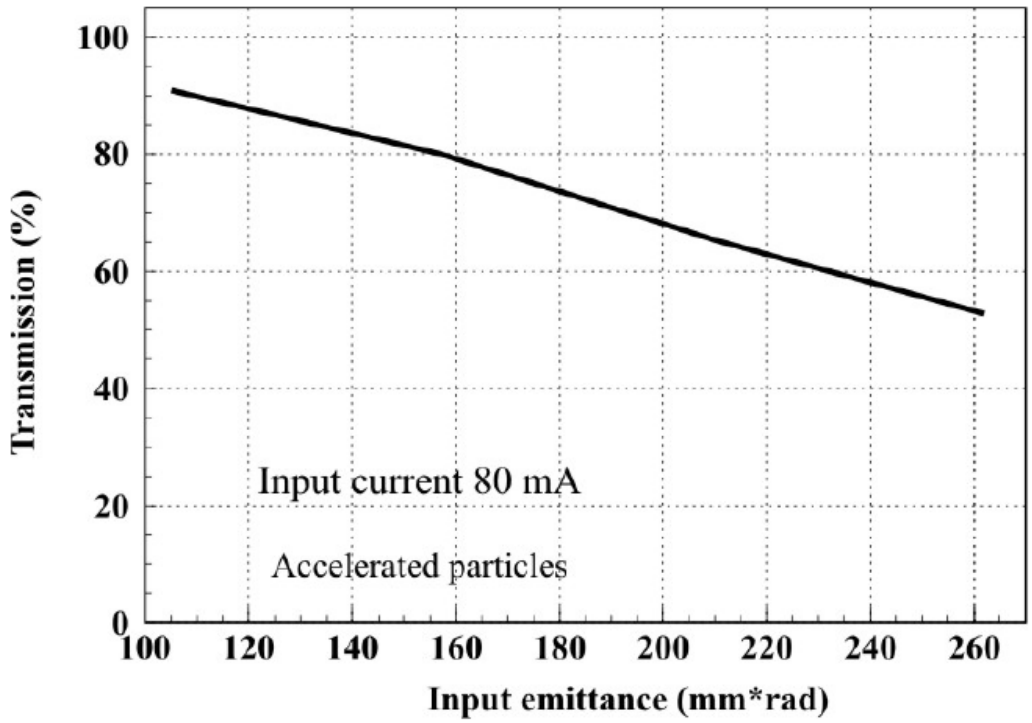

Fig. 2.7.22: RFQ transmission as a function of the total input emittance for a constant current as simulated using the DYNAMION code.

The LEBT output distribution has been accelerated inside the RFQ using DYNAMION and the obtained distribution is shown in Fig. 2.7.23. A transmission of 80% has been achieved being slightly lower as the corresponding value from Fig. 2.7.20 (85%), indicating that the high input emittance is mainly due to few outer halo particles. The final transverse emittances at the RFQ exit are about 1.5 mm mrad. This is in accordance with the brilliance analysis of the LEBT output distribution of Fig. 2.7.48, showing that a current of 80 mA is contained within about 1.5 mm mrad. The brilliance analysis of the RFQ output distribution is shown in Fig. 2.7.24. Comparing the two brilliances leads to the conclusion that there is almost no dilution in beam brilliance during acceleration in the RFQ even for highest input current. Tab. 2.7.7 summarizes the beam parameters at the RFQ exit.

The preceding studies did not include any imperfections with respect to applied voltage and/or fabrication errors. Concerning the applied voltage the report [12] as well as the publication presenting the design [8] showed that there is robustness, i.e. constant transmission, w.r.t. excess of voltage compared to the design value of 80 kV. However, an under-voltage of 5% already causes a 10% drop in transmission of accelerated particles at 80 mA of input current according to DYNAMION simulations.

In order to study the impact of fabrication errors also the DYMAION code will be used. It allows for displacement of single rods along the RFQ cavity as well as for introduction of errors in the applied modulation of the rods. Displacements and imperfections will be studied for 20 µm and for 50 µm. Results are expected to be available at the end of January 2010.

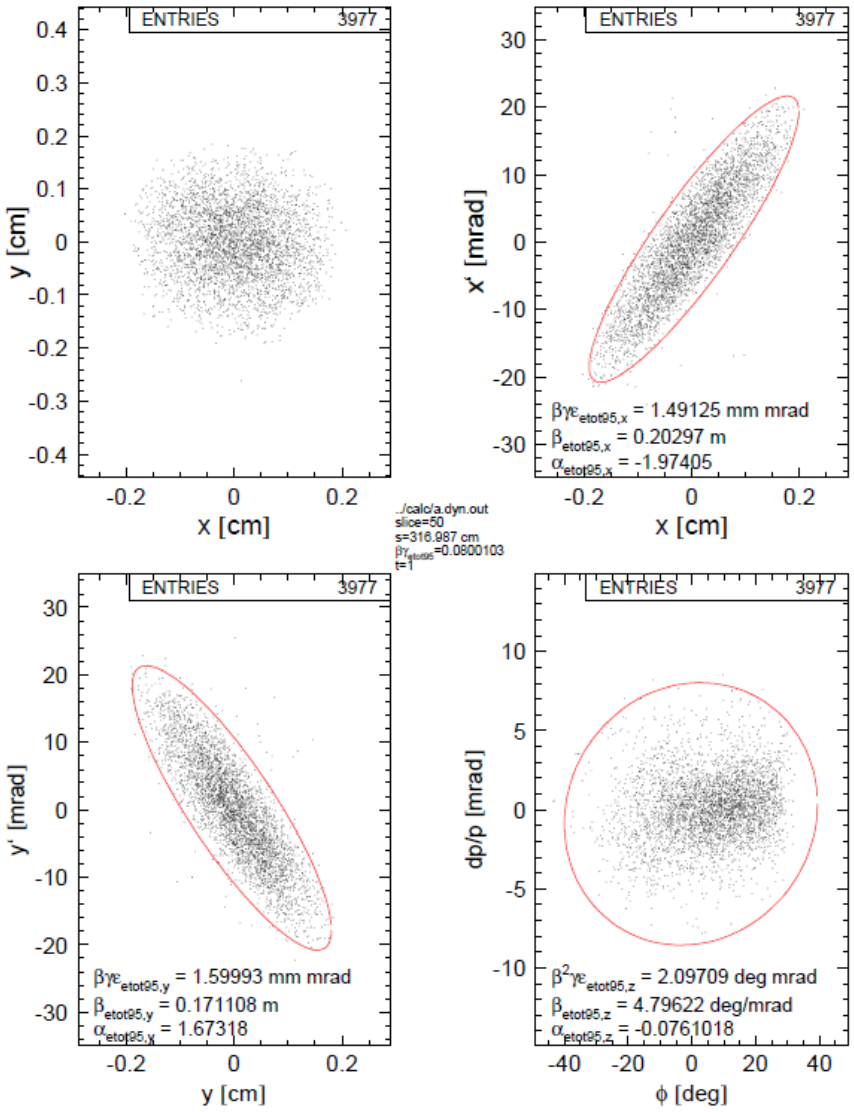

Fig. 2.7.23: Distribution at the RFQ exit from end-to-end simulations.

A cold model (352 MHz) of the 4-rod RFQ with eight stems and elliptical electrodes was built [13] in order to verify the results of simulations on the RF-properties (Fig. 2.7.25). It was demonstrated that eventual differences in the voltages of the upper and lower rods could be eliminated by proper adjustment of the stem slope as shown in Fig. 2.7.26. The closest parasitic oscillation mode was found to be a dipole mode at 379 MHz.
For inductive frequency tuning one plunger will be used as shown Fig. 2.7.25. Each of them can be moved with a range of 70 mm. Simulations using a model of 19 cells with one single tuner confirmed a linear behaviour of 4 kHz/mm.

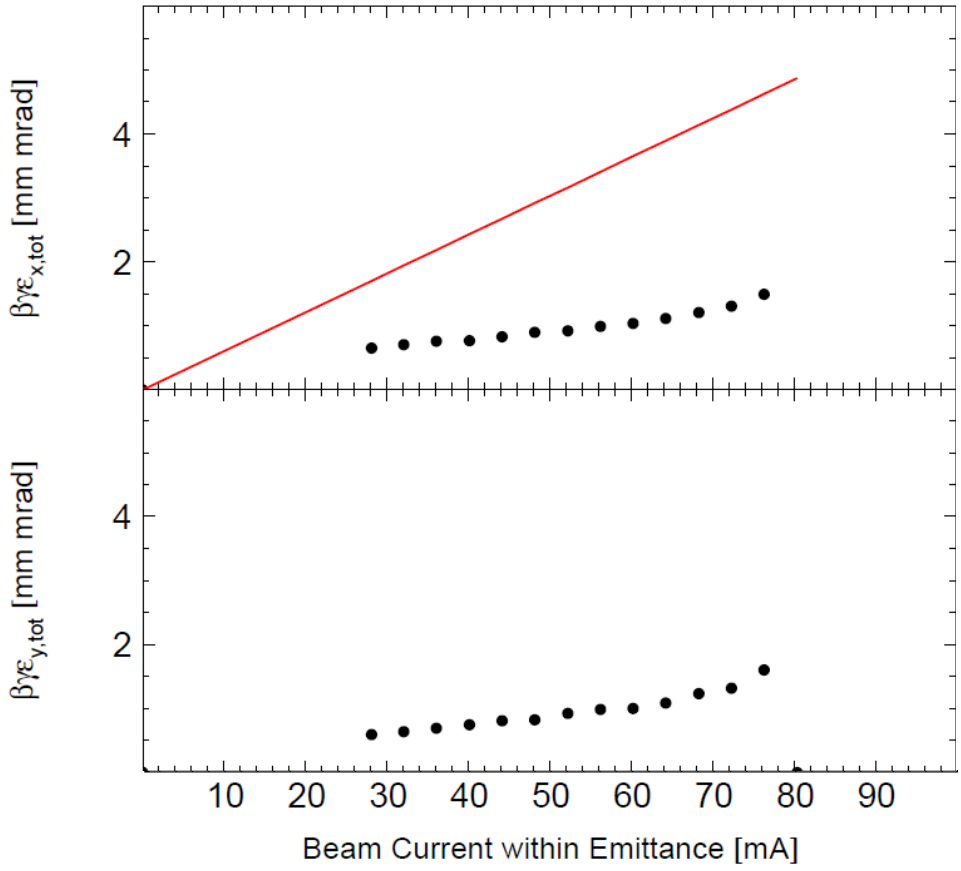

Fig. 2.7.24: Normalized total emittance as function of the beam current confined by the emittance at the exit of the RFQ. The required brilliance at the SIS18 is indicated by a red line.

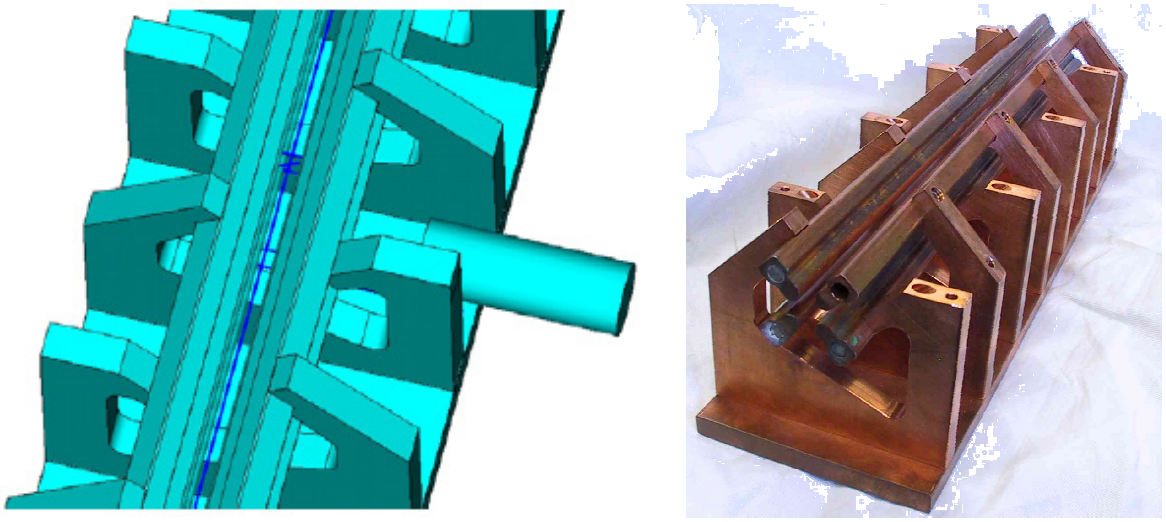

Fig. 2.7.25: Model of the RFQ (352 MHz) as used for the simulations with Microwave Studio® (left) including tuning and real model built at Frankfurt University (right).

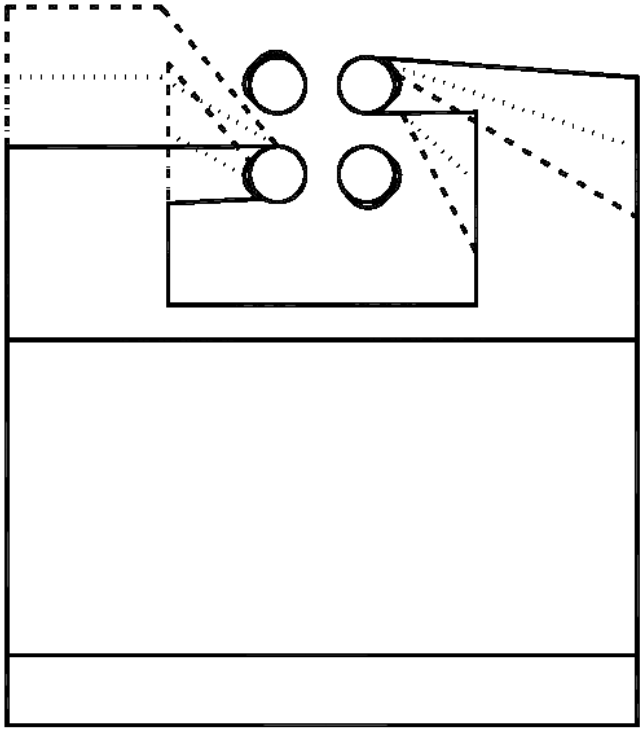

Fig. 2.7.26: Modification (dotted) of the stems for the 4-rod RFQ w.r.t. the geometry used at lower frequencies of about 200 MHz (solid).

Table 2.7.7: Parameters of the RFQ cavity types for the proton linac as achieved in end-to-end simulations. The quoted output emittances enclose 95% of the accelerated output particles.

Parameter	**4-rod RFQ**
input energy	0.095 MeV
input current	100 mA
input emittance (transv., norm., tot.)	2.5 mm mrad
frequency	325.224 MHz
output energy	3.0 MeV
total output current	80.4 mA
output emitt. (transv., norm., tot., 95%)	1.5 / 1.6 mm mrad
output emittance (long., tot, 95%)	2000 keV deg
cavity Q_0-value	3100
distance to closest mode	54 MHz
total RF-input power	0.74 MW
electrode voltage	80 kV
max. electric field strength	34.7 MV/m = 1.94 E_k
aperture radius	2.4 – 3.8 mm
length	3.2 m (214 cells)

2.7.4.3 Re-Bunchers

Three re-bunchers will be used along the linac, all of them require less than 50 kW of RF-power. The first one is needed to longitudinally match the beam from the RFQ to the first CH-cavity [14] of the DTL. The longitudinal dynamics along the DTL is based on the KONUS principle [2], which requires a small phase spread at the entrance to the cavity. The space between the RFQ and the first CH-cavity must house two quadrupoles, a steerer, a phase probe, and a beam current monitor. Without a re-buncher the longitudinal drift would result in too long bunches at the DTL entry. The re-buncher is a two-gap cavity.

A second re-buncher with four gaps is integrated into the extended diagnostic section. It mitigates de-bunching along this prolonged longitudinal drift. Finally, it will serve as an additional tool for machine operation. Operating the re-buncher at phases different from 90° will allow for slight energy variation prior two injection into the second DTL section.

The third re-buncher has six gaps and it is placed in the existing transfer channel from the UNILAC to the SIS18. Its purpose is to tilt the longitudinal phase space distribution in order to minimize the momentum spread for a given longitudinal emittance. The re-bunchers cavity type corresponds to the type for the CH-DTL (see following chapter).

2.7.4.4 CH-Cavities

The drift tube linac will comprise 12 CH-cavities grouped to six pairs. Each pair comprises two RF-coupled cavities as shown in Figs. 2.7.3 and 2.7.27. An RF-coupled pair of CH-cavities will be called CCH in the following. The distribution of the electromagnetic fields inside a CCH was simulated with Microwave Studio®. Configurations of the electric and the magnetic field are shown in Fig. 2.7.27. The polarity of the electric field inside one cavity alternates from gap to gap while it is equal in the subsequent gaps enclosing the central drift tube. This enlarged drift tube represents the RF-coupling transition between the two cavities forming the pair and it will house a focusing quadrupole triplet. Inductive RF-coupling into the cavity pair will be performed opposite to the stem that supports this centre drift tube.

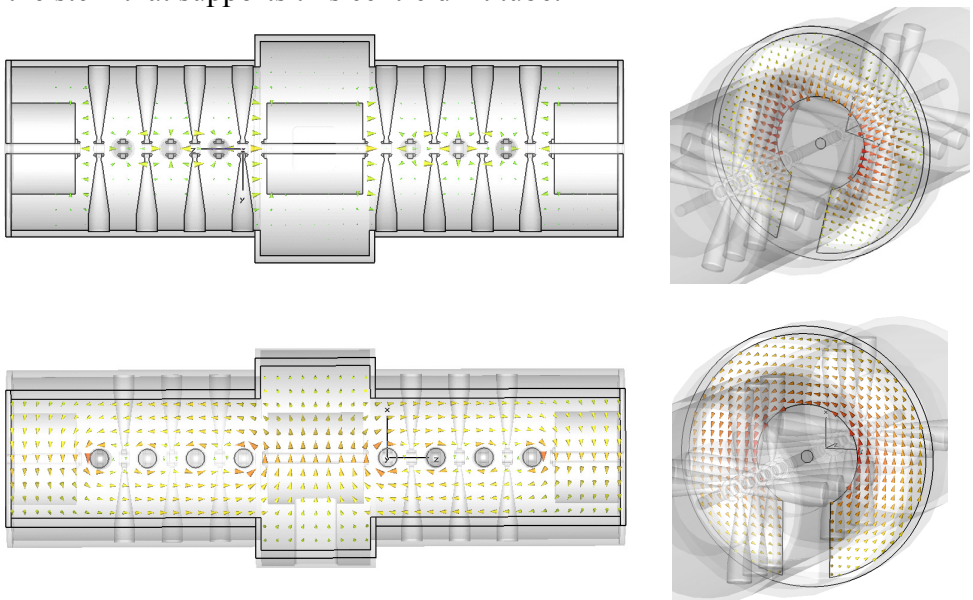

Figure 2.7.27: Distribution of the electric (upper) and the magnetic (lower) field inside a pair of RF-coupled CH-cavities (CCH) as obtained from simulations with Microwave Studio®.

To increase the voltage in the end-cells and to achieve a good flatness of the electric field, the magnetic inductance at the cavity ends is increased. In case of IH-cavities, this is accomplished by large undercuts in the base girder. For the FAIR proton linac design no girder is foreseen and the tuning can be achieved by enlarging those end tubes that do not represent an RF-coupling transition to the neighboring cavity. This drift space can be used as well to host quadruple lenses and beam diagnostic devices.
The stainless steel stems are welded into the cylindrical cavity wall avoiding any screws inside the cavity. As shown in Fig. 2.7.28 the design will result in a good flatness of field distributions together with high effective shunt impedances. Each cavity is equipped with 5 independent tuning plungers and its total weight is well below two tons, such that a fixed crane in the linac tunnel can be avoided.

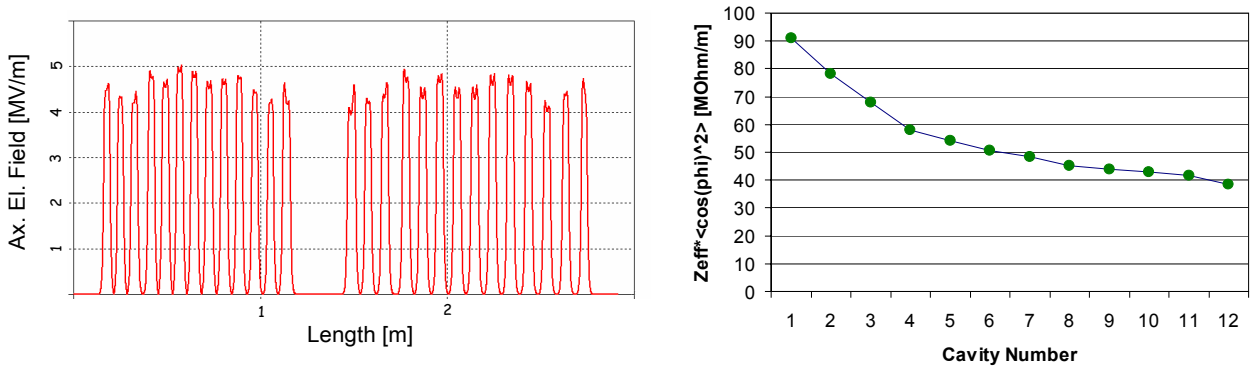

Figure 2.7.28: Left: Axial electric field strength along the CH-cavity as expected from simulations using Microwave Studio®. Right: Effective shunt impedance as function of the beam energy.

The energy gain per cavity ranges from 3.1 to 6.7 MeV and the cavities lengths are between 0.41 m and 2.1 m. Velocity-dependent effective shunt impedances varying from 93 to 41 MΩ/m were achieved in simulations as shown in Fig. 2.7.28. The number of gaps per cavity ranges from 9 to 15 and the Q_0-values are about 17000. The cavity parameters are summarized in Tab. 2.7.8.

Table 2.7.8: Parameters of the 325 MHz RF-cavities of the proton linac, i.e. type, mechanical length, number of gaps, effective shunt impedance, energy gain, peak beam power at 70 mA, peak heat loss power, total peak power, and number of RF-power unit (K for klystron, T for tube amplifier).

Type	L / cm	# Gaps	Rs / MΩ/m	DE / MeV	Pbeam / kW	Ploss / kW	Ptot / kW	Rf-Unit
4-rod RFQ	3,24			2,91	203	537	740	K_1
Re-Buncher_1	*8,06*	*2*	*120*	*0,00*	0	*12*	22	T_1
CH-Cavity_1	40	10	91,1	3,09	216	262	1460	K_2
CH-Cavity_2	68	12	78,2	5,60	392	590		
CH-Cavity_3	96	13	68,0	5,77	404	510	2043	K_3
CH-Cavity_4	124	14	58,0	6,84	479	650		
CH-Cavity_5	152	15	54,2	5,95	417	430	1729	K_4
CH-Cavity_6	168	15	50,5	6,18	433	450		
CH-Cavity_7	182	15	48,3	5,93	415	400	1644	K_5
CH-Cavity_8	194	15	45,1	5,99	419	410		
CH-Cavity_9	206	15	43,9	6,16	431	420	1664	K_6
CH-Cavity_10	202	13	42,9	5,89	412	400		
CH-Cavity_11	211	14	41,7	5,93	415	400	1607	K_7
CH-Cavity_12	203	13	38,6	5,60	392	400		
Re-Buncher_2	*0,72*	*6*	*44,0*	0,00	0	7	7	T_2

RF-coupled CH-cavities have not been built so far and the RF-design as well as the mechanical layout required some R&D effort including a prototype pair of cavities. A cold model single cavity with eight equidistant gaps has been built [15] as shown in Fig 2.7.29. The model has been successfully copper-plated at GSI. Its RF-properties showed excellent agreement with simulations. Especially the measured Q agreed to the calculated one. Generally codes overestimate the Q-values due to inner screws that have been abandoned for the CH-cavity.

In a next step a cold model of a CCH cavity was completed (Fig. 2.7.30). This 2:1 model made from aluminum and messing included a velocity profile. It was used to test the tuning procedure and to investigate its behavior w.r.t. parasite modes. With this model it was demonstrated that sufficient field flatness can be reached as shown in Fig. 2.7.31. The closest parasitic mode was found to be a $\pi/2$-mode 1.5 MHz above the design mode. In this mode the longitudinal magnetic field lines of the coupled cavities are parallel and not anti-parallel as desired. For this reason the $\pi/2$-mode does not couple any more the two cavities through the enlarged drift tube (coupling cell). The mode can be avoiding by just placing the RF-coupling loop inside the coupling cell. Additionally, one of the five plungers will be located in this cell. Measurements at the model confirmed that parasitic mode suppression is successful by applying the described scheme. For details we refer to the dedicated report on the 2:1 model [16].

After successful construction and testing of two different models the design and construction of a fully operational prototype CCH has been started this year. It was decided to choose the second CCH module for doing that, on order to preserve the flexibility to adopt the first model to eventual modifications of the preceding RFQ. The prototype CCH provides acceleration from 11.7 to 24.4 MeV. It has 13 gaps in the first cavity and 14 gaps in the second cavity. The conceptual design is available [17] and the completion of the drawings for construction is expected for March 2010. Figure 2.7.32 shows its layout.

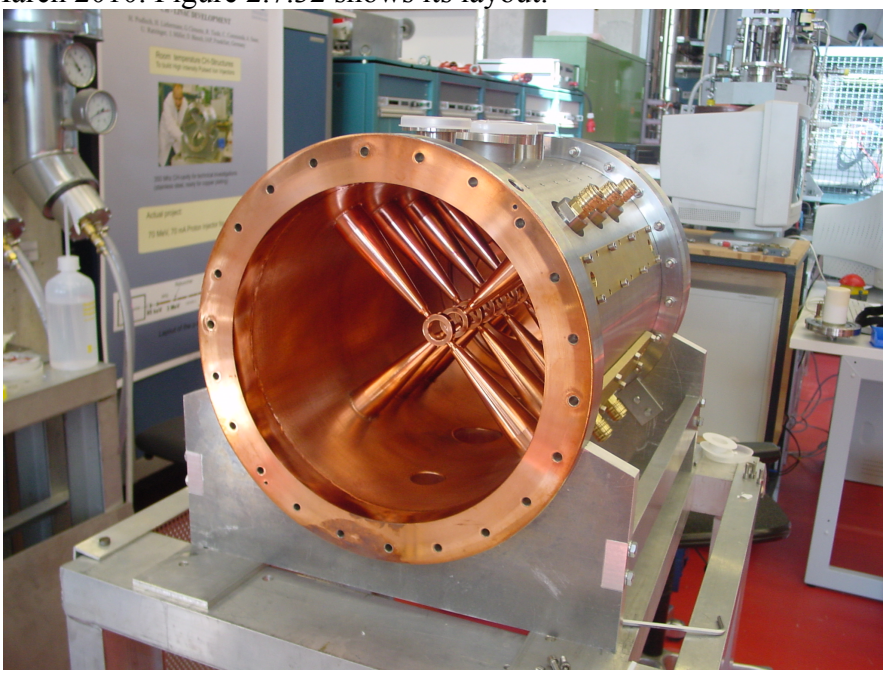

Figure 2.7.29: Cold model of a CH-cavity (314 MHz). Design and construction has been done at University of Frankfurt. The copper plating has been done at GSI.

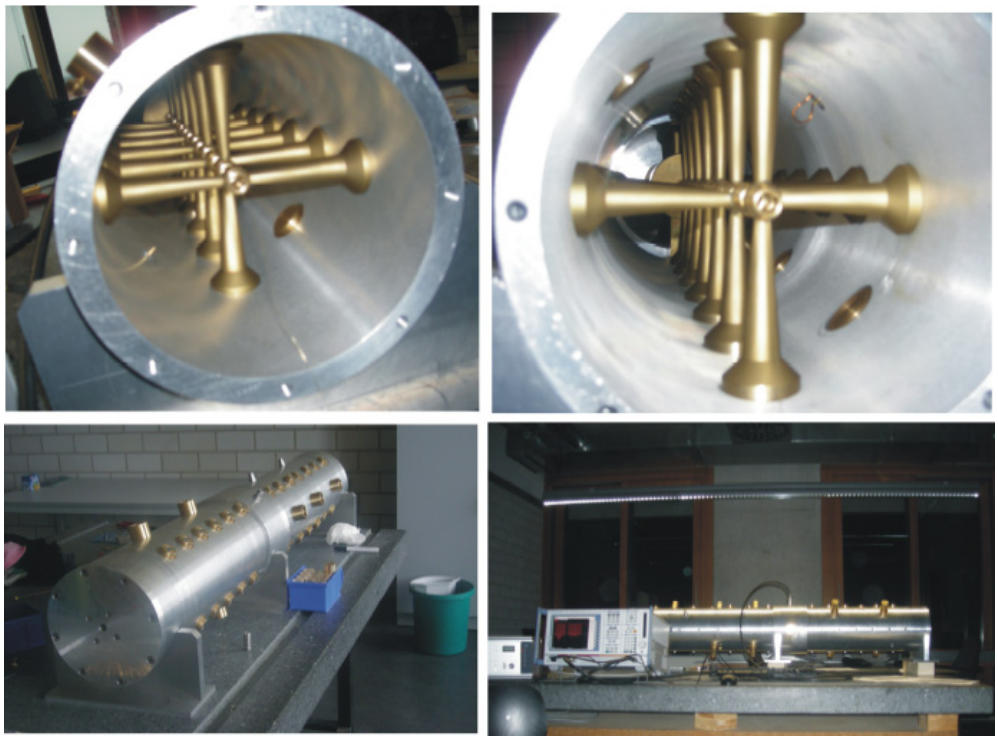

Fig. 2.7.30: 2:1 cold model of a pair of RF-coupled CH-cavities. Design and construction has been done at the University of Frankfurt.

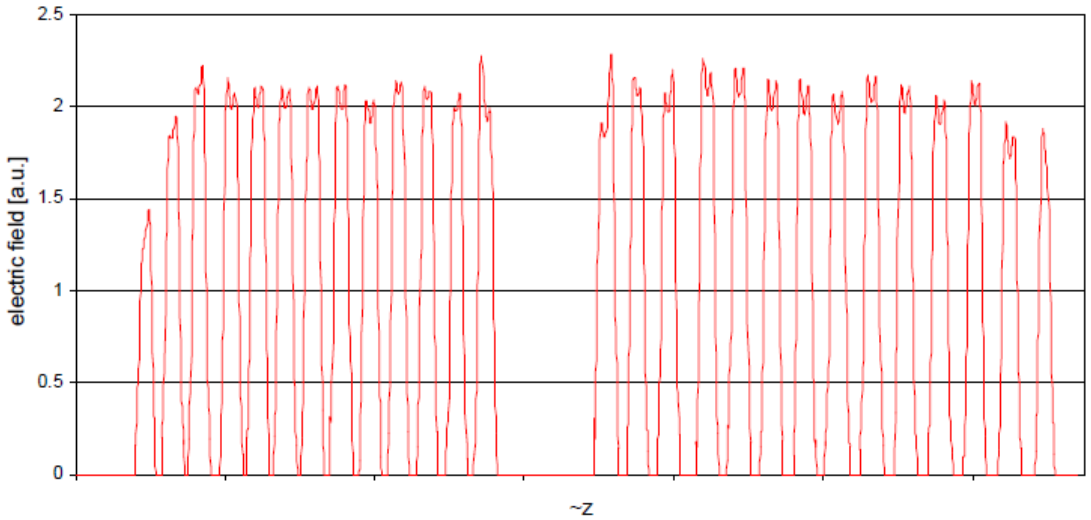

Fig. 2.7.31: Measured filed flatness for the 2:1 cold model of a pair of RF-coupled CH-cavities.

The production of the mantle has been started already. Currently minor changes in the design of the cooling channels along the stems as well as on the support of the coupling cells are included. Prior to final production of the stems and drift tubes from stainless, dummies from aluminum are to be produced since the field flatness tuning is by variation of the drift tube length. The final delivery of the CCH to GSI is expected at the beginning of 2011. At GSI it will be copper-plated. Measurements on its RF-properties at low and high power levels are to be done at the dedicated

RF-test-stand on GSI site. The two DTL sections are built from three CCH modules, respectively. Adjacent modules are screwed directly together such that the two DTL sections form one compact unit each as illustrated in Fig. 2.7.2.

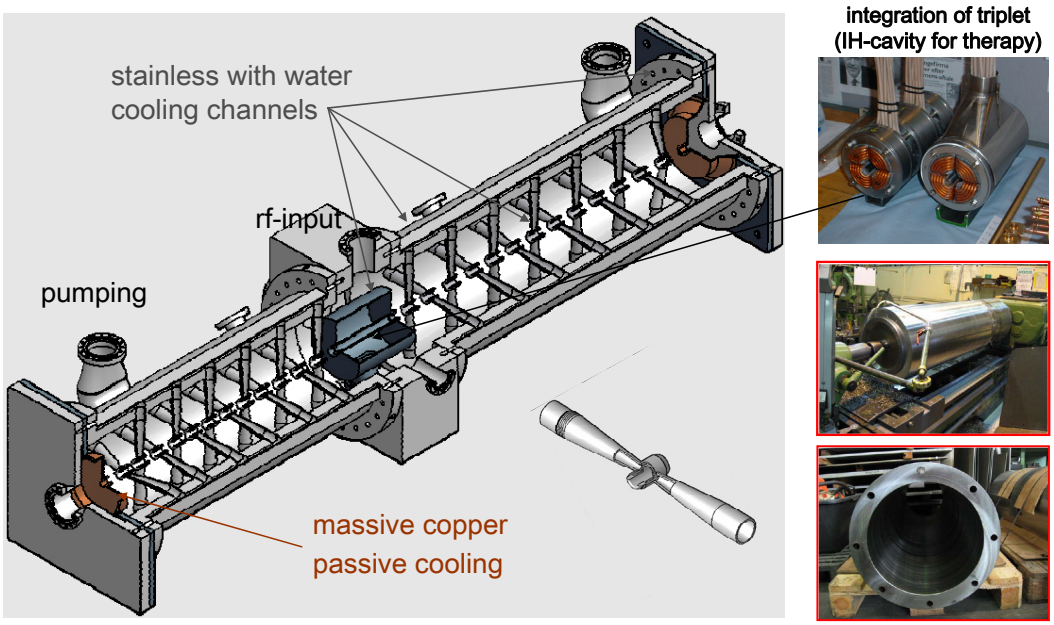

Fig. 2.7.32: Layout of the prototype of the second couples CH-cavity module.

The beam dynamics layout is different from the classical layout of a DTL for an energy of less than 100 MeV. In an Alvarez type DTL each drift tube houses a quadrupole to compensate for the transverse defocusing resulting from acceleration at negative phases from crest. In CH (and IH) type DTLs these quadrupoles are abandoned thus shortening the overall cavity length. As a consequence the rf-crest must be moved away from negative phases to avoid transverse defocusing.

The resulting KONUS [2] focusing scheme distinguishes between the synchronous particle and the centre-of-bunch particle as illustrated in Fig. 2.7.33. Along the first few gaps (2-4) after a triplet the two particles are identical and acceleration is done at about -30° from crest to provide longitudinal focusing. The subsequent drift tube is considerable longer than the preceding ones thus moving the centre-of-bunch phase at the next gap towards positive values. The following gaps and drift tubes a designed for a synchronous phase of 0° and for a synchronous energy that is lower by some few percent w.r.t. the centre-of-bunch particle. Consequently, the centre-of-bunch particles' phase will move backwards from positive values to negative phase values. Its positive energy offset compared to the synchronous particle decreases. If this movement continues infinitely the particle will be lost since the movement is outside of the stable bucket region. Therefore it is stopped at about -30° when the energy offset is zero, i.e. at the entrance to the third quadrant of the separatrix. At this point the bunch enters into the next triplet. After the triplet the next KONUS section starts.

Beam dynamics simulations have been done using the LORASR code developed at Frankfurt University. As input the simulated distribution at the RFQ output has been used. The simulations included the MEBT section comprising a doublet and the first re-buncher. The final distribution at the exit of the last CCH module is plotted in Fig. 2.7.34. The normalized horizontal emittance of 3.8 mm mrad is below the design value of 4.2 mm mrad. Figure 2.7.35 shows the

corresponding brilliance curve.

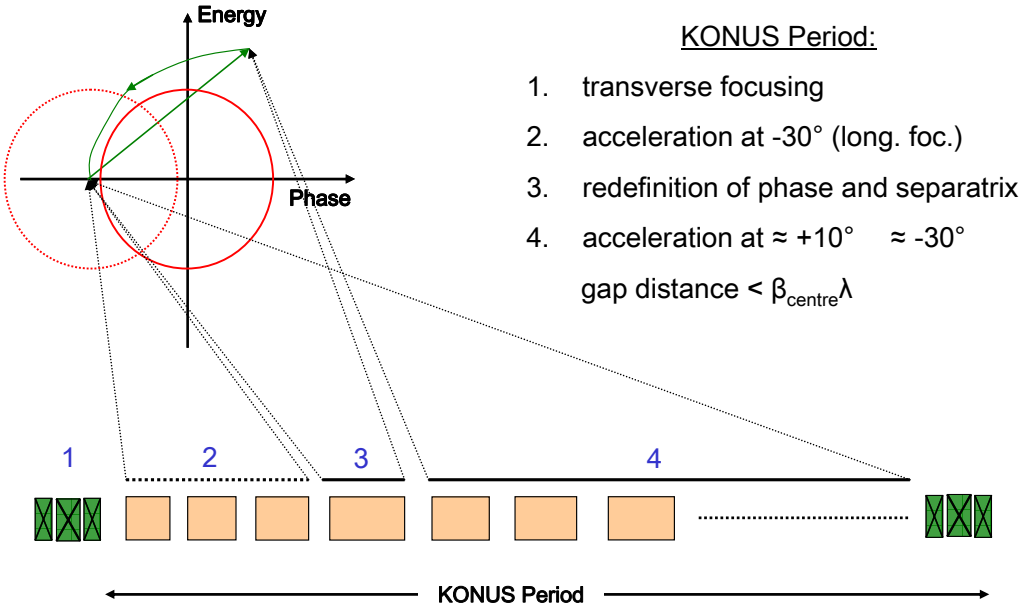

Fig. 2.7.33: Principle of the KONUS focusing scheme as applied in CH-cavities.

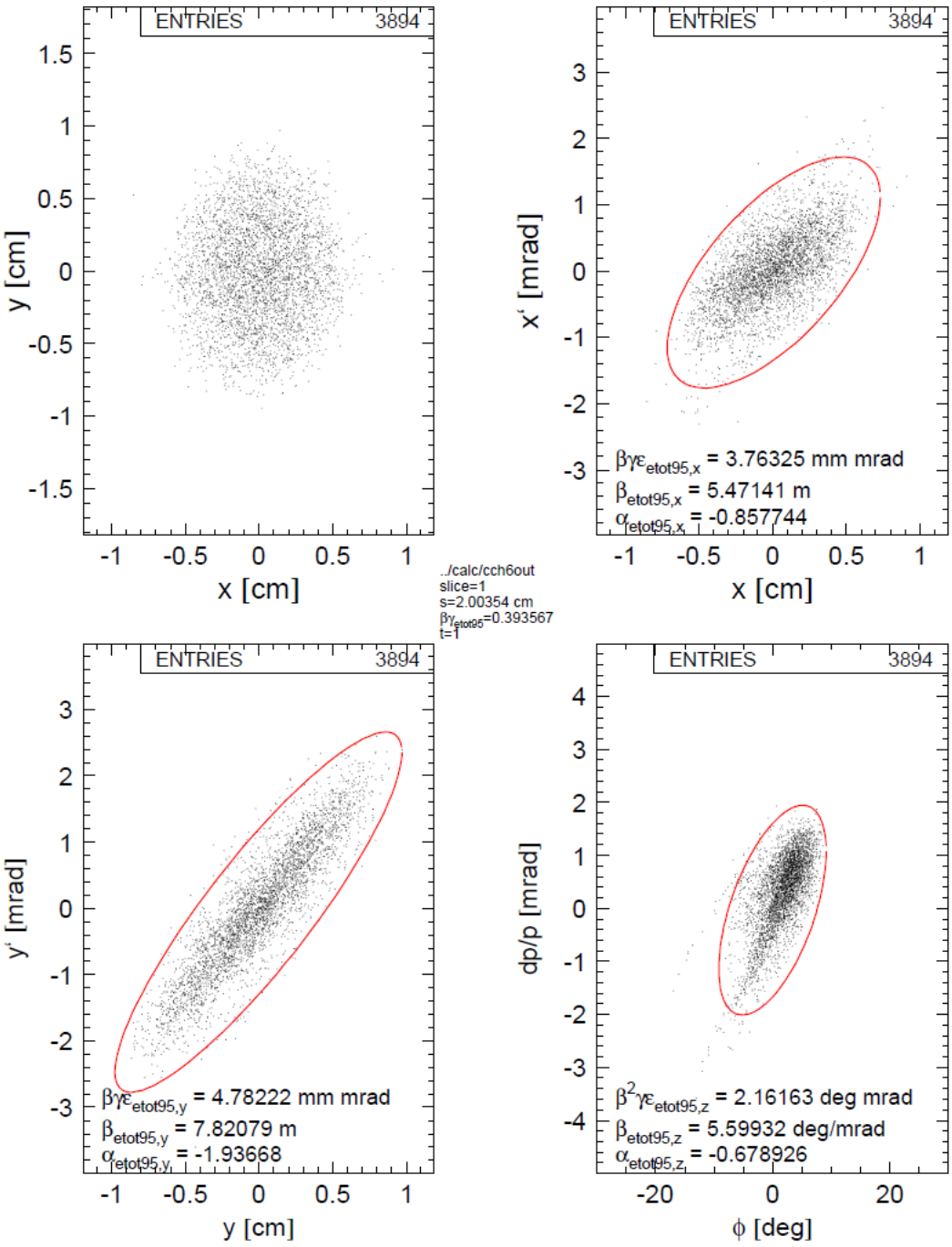

Fig. 2.7.34: Phase space distribution at the exit of the DTL as obtained from end-to-end simulations.

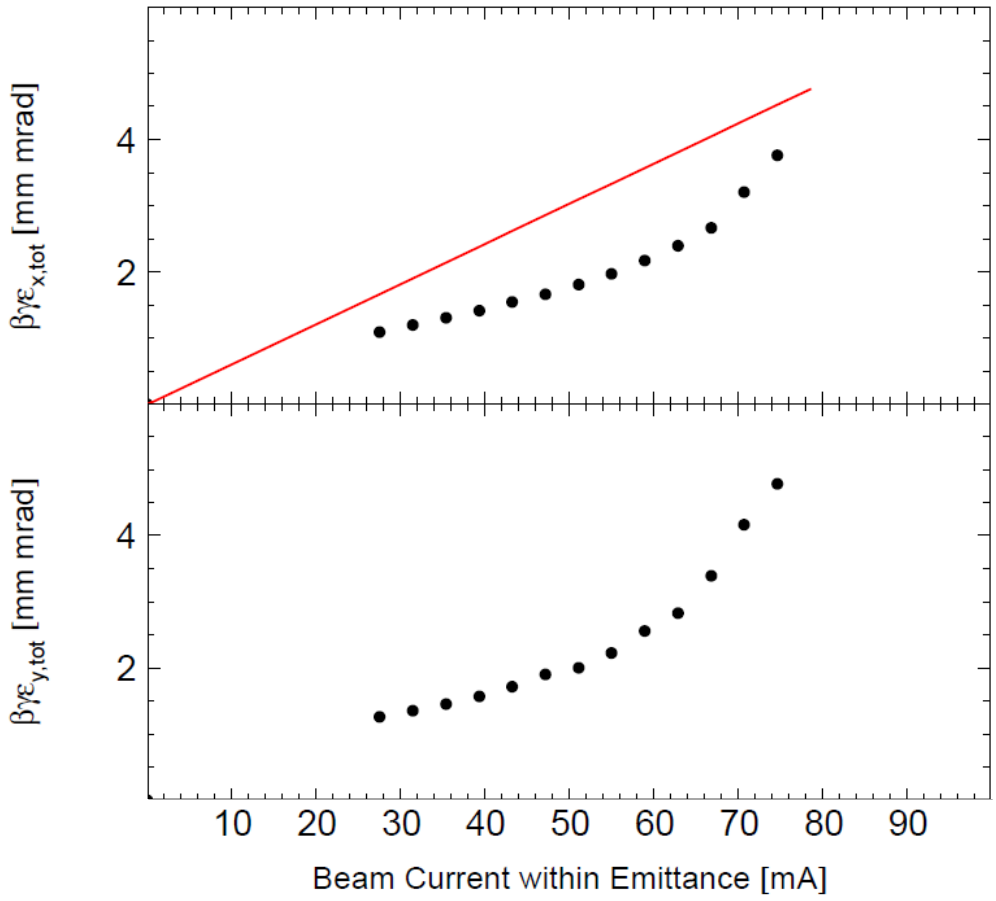

Fig. 2.7.35: Normalized total emittance as a function of the beam current confined by the emittance at the exit of the DTL. The required brilliance at the SIS18 is indicated by a red line.

2.7.6 Beam Diagnostics

The beam diagnostic components are defined as well as their locations along the linac and the beam transport lines (Fig. 2.7.36). Their main parameters are listed in Tab. 2.7.9.

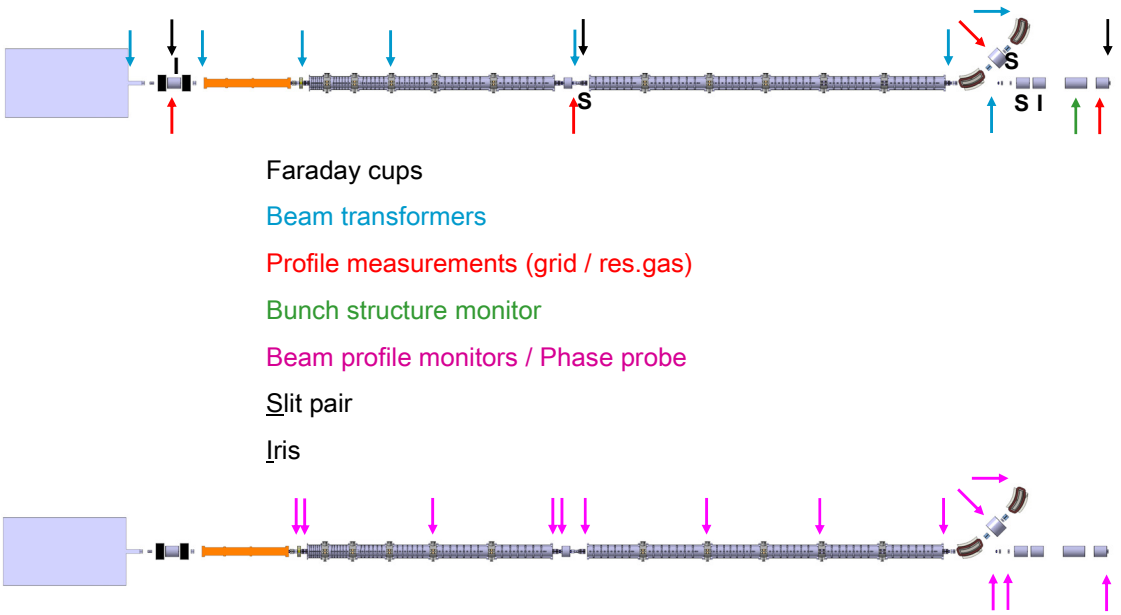

Fig. 2.7.36: Position of beam diagnostic devices along the beam line of the proton linac.

2.7.6.1 Faraday-Cups

The properties of Faraday-cups are well known. Beside the current measurement they also serve as a beam dump for the full beam power (4.9 MW peak, 0.7 kW average). GSI has large experience with the technical realization using a special shaped water-cooled copper block coated with tungsten [18].

2.7.6.2 ACT Beam Transformers

High performance active current transformers (Alternating Current Transformers ACT, Fig. 2.7.37) were developed and are in operation at the UNILAC [19] since several years. They are well suited for beam pulse lengths from a few µs up to the maximum design length of 36 µs offering high sensitivity and large dynamic range. For readout and presentation a versatile data acquisition system is in preparation for the UNILAC. This system can be duplicated for the proton linac.

2.7.6.3 Profile Measurements (Grid)

At GSI Secondary EMission (SEM)-grids are used very frequently. The technology of the mechanical construction as well as the sensitive pre-amplifier electronics is well developed. SEM-grids offer a large dynamic range and in connection with slits they serve as transverse emittance measurement devices. For cost reduction a re-design for the electronics is under preparation using modern multi-channel integrated circuits and standard digital equipment.

Table 2.7.9: Beam diagnostic devices of the proton linac, their locations, numbers to be used, installation lengths (not including the respective vacuum chamber), and aperture radii.

Device	Location	#	Length / mm	Aperture Radius / mm
Faraday Cup	LEBT	1	150	80
Faraday Cup	DTL	1	150	15
Faraday Cup	Dump	1	150	33
ACT Beam Transformator	LEBT	2	100	80
ACT Beam Transformator	MEBT, DTL(3)	4	100	15
ACT Beam Transformator	Transfer Channel	1	100	50
ACT Beam Transformator	Dump	1	100	33
Profile Measurement (grid)	LEBT	1	150	80
Profile Measurement (grid)	DLT	1	150	15
Profile Measurement (grid)	Dump	1	150	33
Profile Measurement (grid)	Inflection	1	150	20
Profile Measurement (residual gas)	*LEBT*	*1*	*500*	*80*
Profile Measurement (residual gas)	*DLT*	*1*	*500*	*15*
Profile Measurement (residual gas)	*Dump*	*1*	*500*	*33*
Profile Measurement (residual gas)	*Inflection*	*1*	*500*	*20*
Beam Position Monitor / Phase Probe	MEBT(2), DTL(7)	9	100	15
Beam Position Monitor / Phase Probe	Inflection	1	100	20
Beam Position Monitor / Phase Probe	Dump	3	100	33
Beam Position Monitor / Phase Probe	Transfer Channel	1	100	50
Bunch Structure Monitor	Dump	1	1000	33
Slit Pair	DTL	1	150	15
Slit Pair	Dump	1	150	33
Slit Pair	Inflection	1	150	20
Iris	LEBT	1	150	80
Iris	Dump	1	150	20

Figure 2.7.37: The ACT system installed at the UNILAC.

2.7.6.4 Profile Measurements (Residual Gas)

The high beam power might not permit the use of SEM-grids for profile measurements. Therefore the use of non-destructive techniques, like the measurement of the profile by Beam Induced Fluorescence (BIF), is under consideration. This technique was also successfully demonstrated for protons at the IPHI front-end at CEA/Saclay [20,21]. Encouraged by the FAIR Technical Advisory Committee it is planned to profit from this development [22]. The mechanical length of the set-up of about 500 mm does not indicate installation of more than one unit within the DTL. Although GSI has experience with BIF profile measurements for ions [23], R&D is needed especially with respect to the extension of this technique to protons.

2.7.6.5 Beam Position Monitors & Phase Probes

Beside the current the beam position will be monitored permanently. Capacitive Beam Position Monitors (BPM) will be used, forming a compact mechanical unit together with the phase probes. The aimed resolution is 1° in phase and 0.1 mm in space. Many of these devices will be installed inside the extended drift tubes of the CH-cavities as indicated in Fig. 2.7.38. Combinations of BPM and phase probes are used at the GSI UNILAC. But due to the higher accelerating frequency of the proton linac compared to the UNILAC (108 MHz), some R&D is still required to develop the devices including the front-end electronics to provide sufficiently large bandwidth. Recently a joint R&D activity has been established with CEA/Saclay. A major concern is the penetration of primary rf-power from the cavities into the extended drift tubes, although the wavelength is beyond cut-off. One remedy might be the insertion of a ferrite iris for additional damping of the parasite fields. Detailed simulations on this penetration have been started recently. Another concern is the cabeling under the restriction of limited space within the tubes.
The probe design represents an overlap of many interfaces within the linac project. Very close and well-coordinated collaboration is required among the layout of beam dynamics, cavities, magnets, and the probes itself. For time being the conceptual layout of the probes foresees four knobs for capacitive pick-up as shown in Fig. 2.7.39. The knobs are welded directly onto the

beam pipe implying that for units inside drift tubes, the complete set-up comprising drift tube, beam pipe, probe, and magnets must be fabricated together by one single manufacturer. After production this unit is integrated into the cavity.

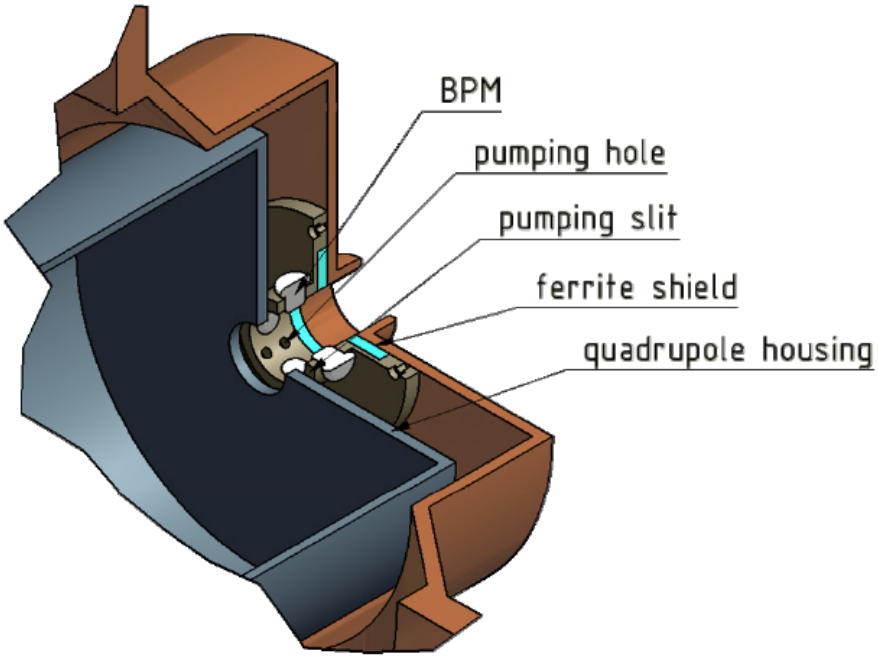

Fig. 2.7.38: Integration of BPM / phase probes inside extended drift tubes of the cavities.

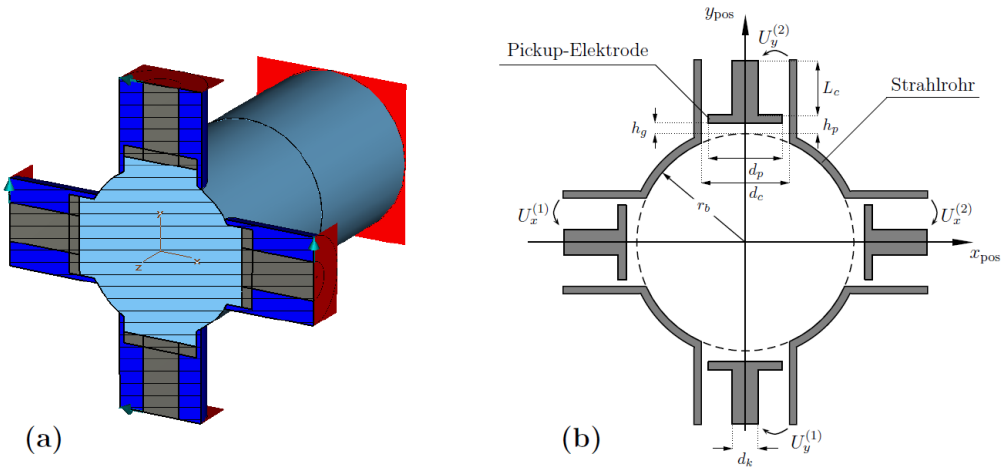

Fig. 2.7.39: Schematic view of the BPM / phase probes comprising for capacitive pick-up knobs.

First simulations on the signal pick-up performance of the knobs have been done in 2008 neglecting the penetration of primary rf-power [24]. The resolution has been investigated as function of the beam energy and of the harmonic number of the bunch frequency as demonstrated in Fig. 2.7.40. However, as mentioned above further R&D is required and has been initiated.

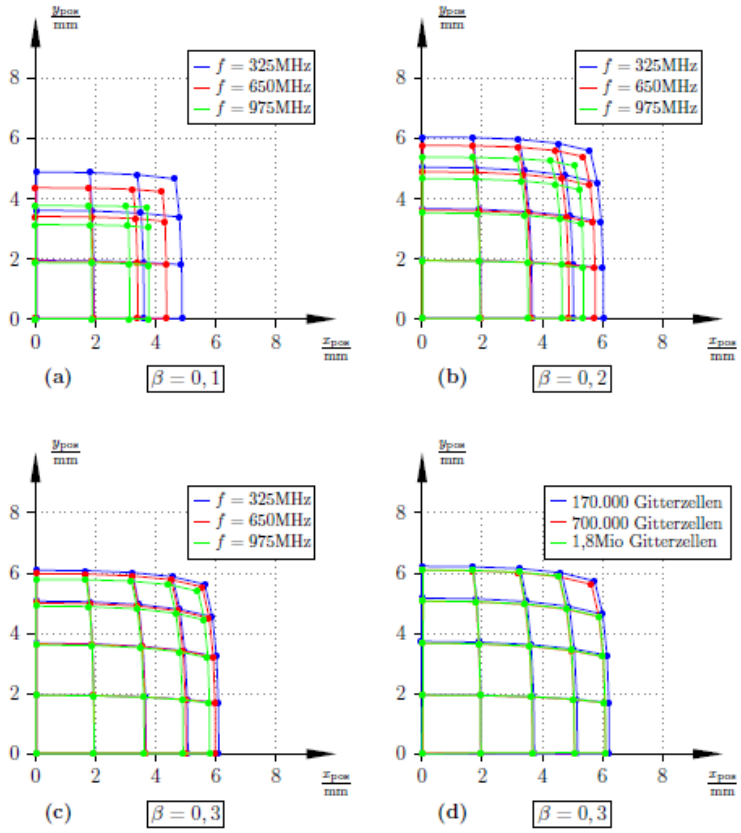

Fig. 2.7.40: Resolution in space of the BPMs for different beam energies and bunch harmonics.

2.7.6.6 Bunch Structure Monitor

A novel non-intersecting method for the high resolution bunch structure measurement was developed at GSI, where the time spectrum of secondary electrons from the residual gas reflects the bunch structure [25]. First promising tests were performed at the UNILAC. A phase resolution of 2^{o} has been achieved with this non-destructive method. This complex system has to be copied and modified for the higher frequency of the proton linac. It will be used during the section-wise commissioning of the linac. Concerning the data acquisition system further developments are required transforming this experimental device into an operating tool.

2.7.6.7-8 Slit Pairs and Irises

Pairs of slits and irises are required for transverse beam emittance measurements or beam size scraping. The slit diaphragm is made of tungsten coated copper and it is water-cooled and driven by a precise stepping motor. Using stepping motor driven horizontal and vertical slits and a SEM-grid with 0.5 mm wire spacing, the transverse emittances can be determined. This technique and its offline analysis are well established. Due to the intersecting material the macro-pulse length has to be reduced during the measurements. The iris between the LEBT solenoids will serve to reduce the beam current in case it is required by the users.

2.7.7 Vacuum

The layout of the vacuum system for the proton linac is straight forward in comparison to the synchrotrons and storage rings. Table 2.7.10 lists the required components.

Table 2.7.10: Components of the vacuum system for the proton linac and their respective numbers to be used. Their locations are given in the text.

Component	Number
Turbo Pump 2000 l/sec	1
Turbo Pump 500 l/sec	9
Ion Pump	34
Sector Valve	7
Fast Valve	2
Pressure Meas. Unit	15
Diagnostic Box	6

2.7.7.1.1 Pumps

One powerful turbo pump (2000 l/sec, oil-free) will be installed at the proton source. The other pumps provide a pumping speed of 500 l/sec. The LEBT section is equipped with one turbo- and with two ion pumps. RF-cavities are pumped with one ion-pump per meter in average, thus that the number of pumps is given by the integer part of the sum over all cavity lengths plus one. The RFQ and the two re-bunchers are pumped by a single turbo pump at each device. The CH-cavities No.1 to No.6 are grouped to one turbo-pump section, similarly the cavities No.7 to No.10 and No.11 to No.12, respectively. The extended diagnostic section after cavity No.6 needs a turbo- and an ion pump. Two ion- and a single turbo pump are installed along the inflection into the transfer channel to the SIS18 and along the beam line to the proton beam dump, respectively.

2.7.7.1.3 Valves

Seven vacuum sections, separated by seven sector valves, comprise the proton linac beam line as drawn in Fig. 2.7.41. Since the overall linac is short w.r.t. synchrotrons or rings just two fast valves are installed along the linac: one to protect the linac w.r.t. the transfer line from the UNILAC to the SIS18 and one to protect the proton source.

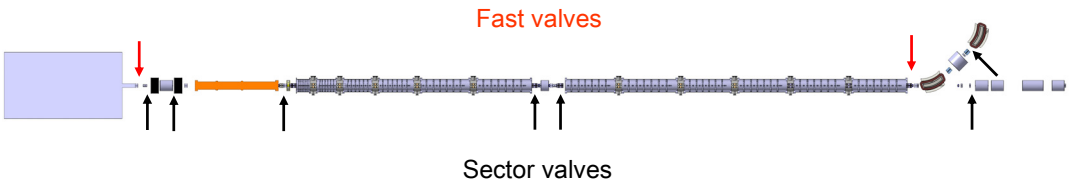

Figure 2.7.41: Position of valves along the beam line of the proton linac.

2.7.7.1.5 Pressure Measurement Units

Dedicated pressure measurement probes are installed in each RF-cavity.

2.7.8 Proton Source and LEBT

An ECR type proton source will be used for the FAIR proton linac. The extraction energy is 95 keV and the proton fraction must be at least 100 mA. Joint measurements of CEA, GSI, and University of Frankfurt on the beam quality of the SILHI ECR source [20] have been done [26]. It was shown that a modified version of the SILHI, i.e. optimized for pulsed operation, could be used for the FAIR proton linac. The stability of the source as well as the reproducibility of its beam parameters was impressive. As an example two different measurements of the vertical emittance close behind the virtual injection point into the RFQ are shown in Fig. 2.7.42. Both measurements were done with the same source & LEBT settings, but they are separated by four days including an opening of the plasma chamber, and employed two different data acquisition systems. The measured phase space distribution includes all fractions of the beam as H_2, H^+, H_2^+, and H_3^+.

The SILHI uses a penthode extraction system as shown in Fig. 2.7.43. Prior to the repeller electrode there is no space charge compensation. Afterwards a compensation of about 75% is assumed. The peak electric field of 97.5 kV/cm appears between the intermediate electrode and the first ground electrode. A value of 100 kV/cm is commonly considered as a reasonable limit. Further optimization of the electrode system might be achieved by moving the repeller closer to the first ground electrode.

Within the French-German collaboration CEA/Saclay currently investigates the option to omit the first grounding electrode, i.e. using a 4-electrode extraction system instead. Such an extraction system is foreseen to be used for the IFMIF project (Fig. 2.7.44) [27]. Since omission of this sparking-protecting electrode might harm the system reliability, the extraction system will be designed such that it can be exchanged within few days even after commissioning of the complete source set-up. Simulations of the beam extraction use the 2d-code AXE-INP starting from the plasma knee to the final ground electrode.

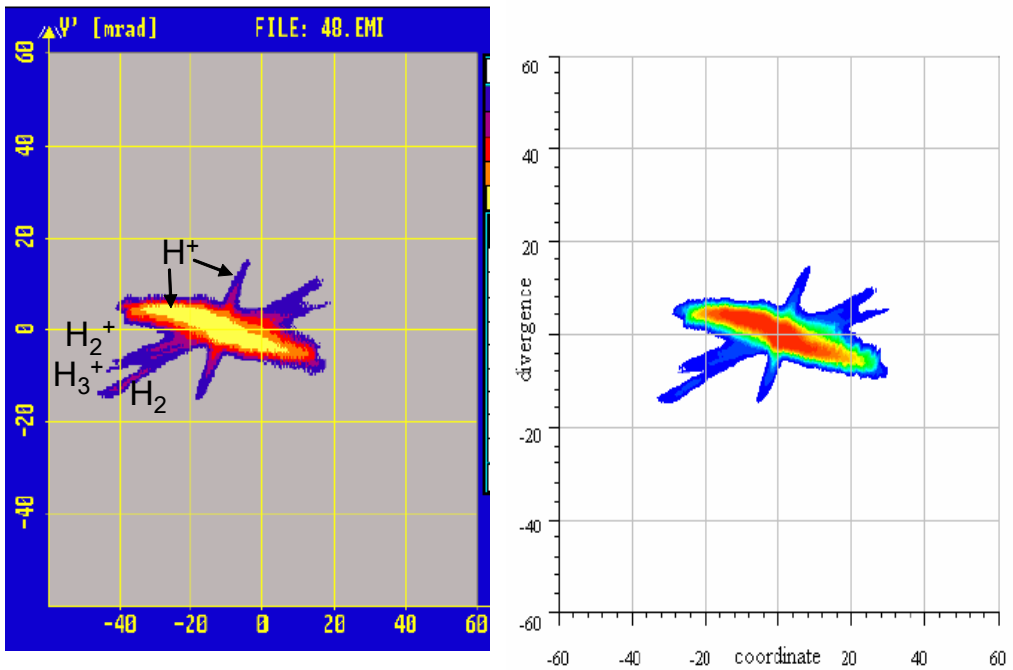

Figure 2.7.42: Two independent measurements of the vertical beam emittance at the exit of the SILHI LEBT.

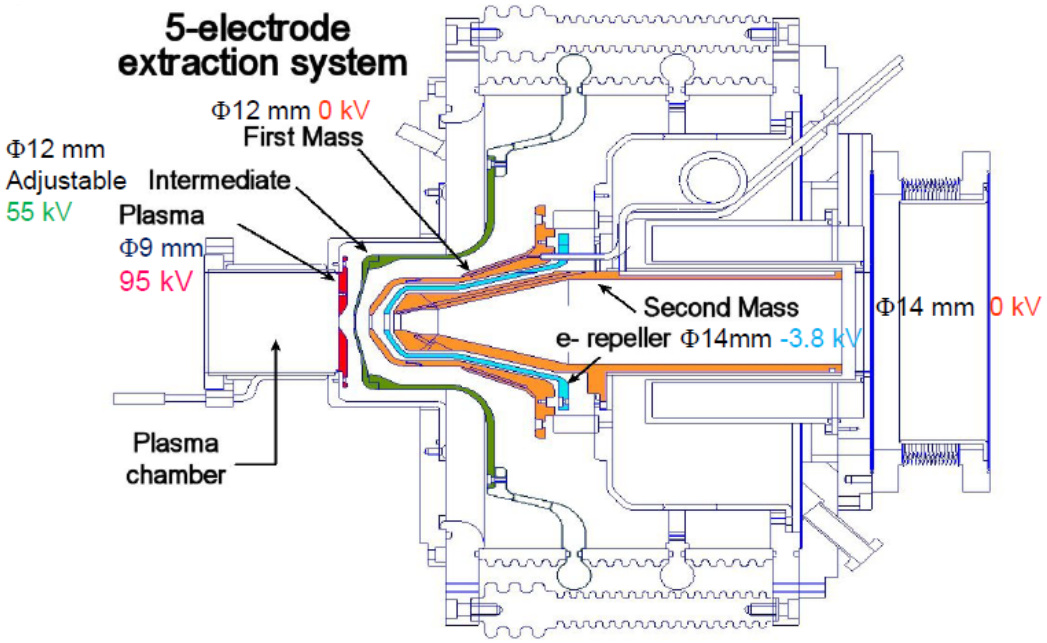

Figure 2.7.43: Penthode extraction system currently installed at the SILHI at CEA/Saclay.

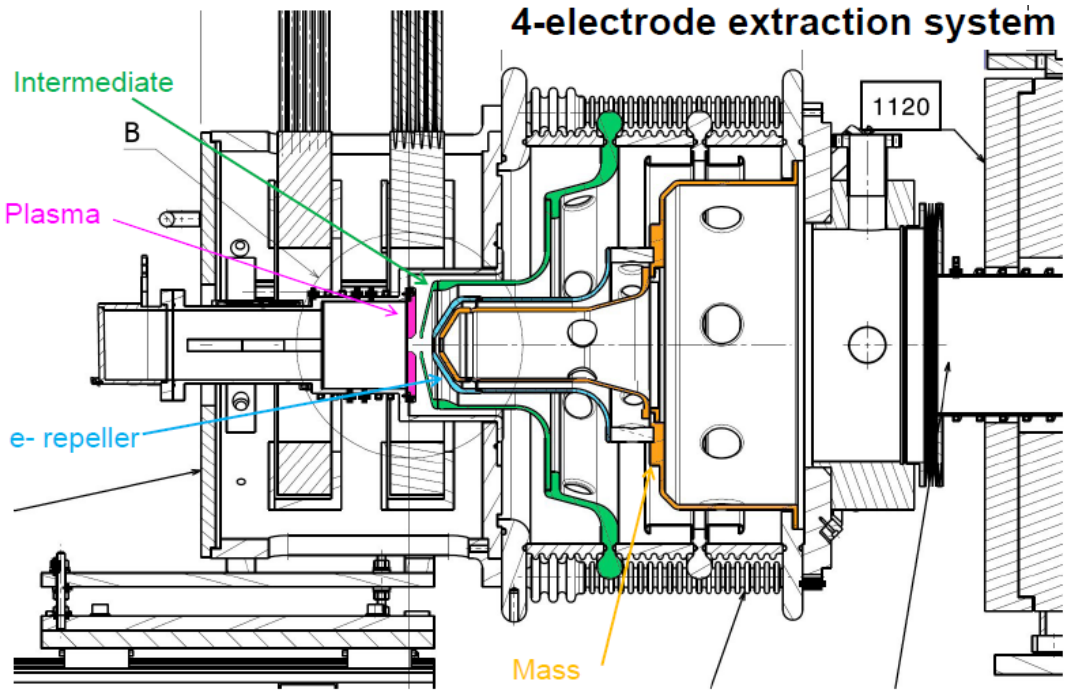

Figure 2.7.44: Four-electrode extraction system from the ECR source for IFMIF.

The design of the LEBT is done at CEA/Saclay as well. It is based on the layout of the IFMIF LEBT (Fig. 2.7.45). The engineering design of its two solenoids including the integrated steerers will be copied for the FAIR proton linac. Minor adoptions to the FAIR common technical

guidelines are currently employed. The same applies to the vacuum system of the set-up.

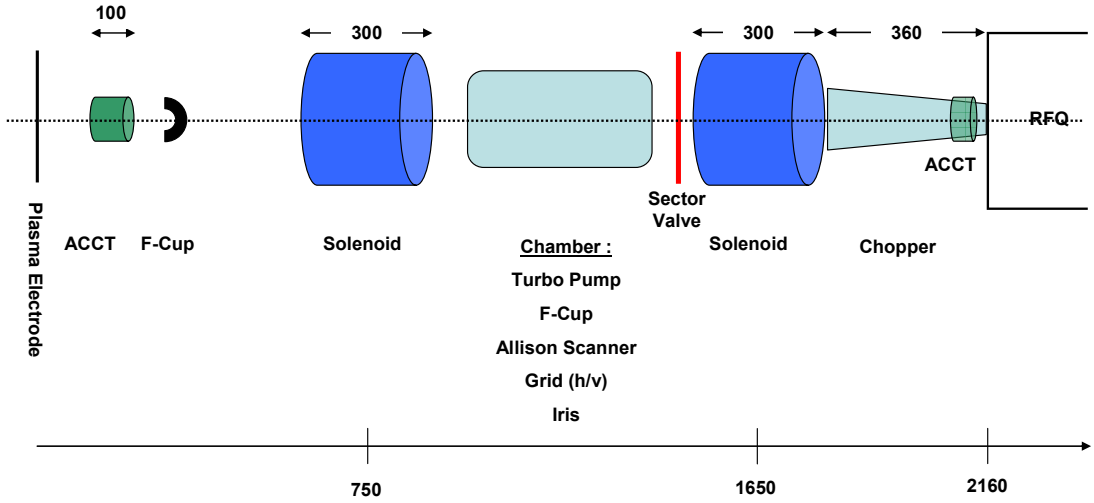

Figure 2.7.45: Conceptual layout of the LEBT including the diagnostic devices.

Beam dynamics calculations use two codes in an iterative procedure: the code TraceWin for particle tracking with space charge and the code SOLMAXP for calculation of the space charge compensation as a function of time and position.
A first calculation is made with TraceWin, considering around 75% of homogeneous space charge neutralization. It serves for initial estimation of the beam transport and focalization that meet the required Twiss parameters for the injection in the RFQ, i.e. the solenoid magnetic field values. Then a calculation is made with SOLMAXP, simulating beam's particles collisions (neutralization and ionization) with the residual gas components using a Monte-Carlo algorithm. SOLMAXP runs until the steady-state of the space charge compensation is reached. The code provides the particle distribution (ions, electrons, neutral atoms) and the electric field map derived from the potential created by the space charge along the beam line (Fig. 2.7.46). This model includes the residual gas properties and the full electrode geometry from the plasma extraction until the chopper entry. The chopper electrodes will be included in a further step.
For the next TraceWin calculation, the space charge electric field map from SOLMAXP is superimposed to those of the beam line elements. During the next TraceWin optimization process, the optics parameters are modified. Consequently, the space charge compensation should vary, due to the new particle distribution. Accordingly, another simulation has to be done with SOLMAXP. After a few iterations between the two codes convergence is reached.

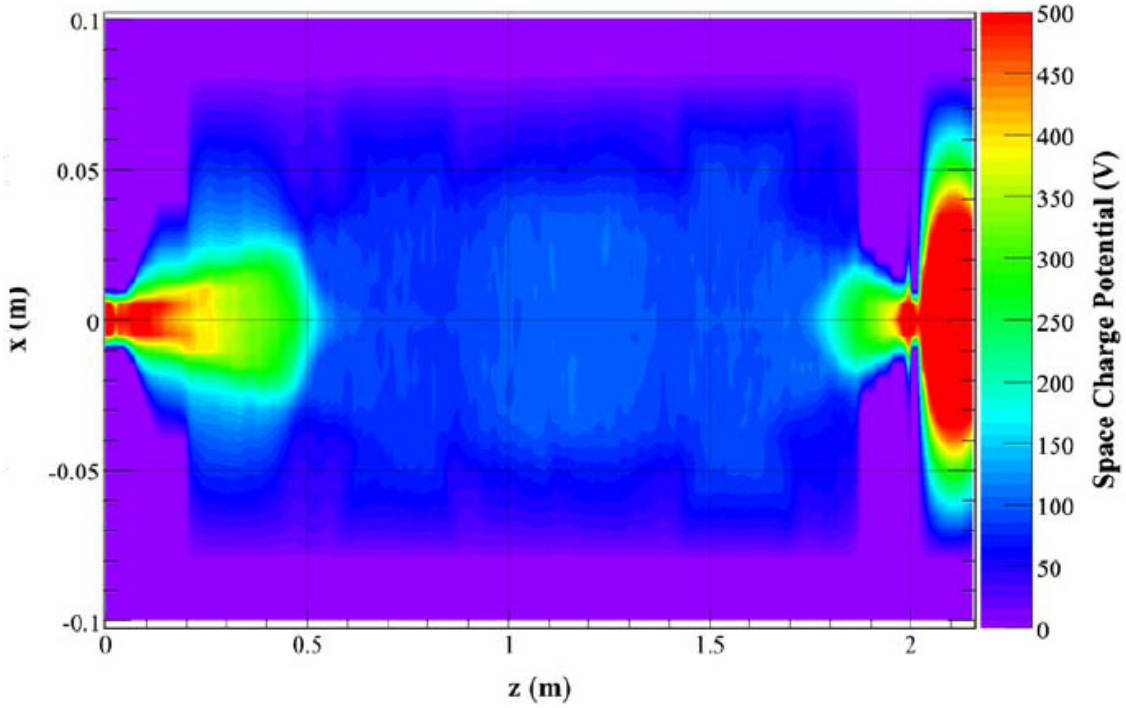

Figure 2.7.46: Map of the space charge potential calculated with SOLMAPX. The cut level is 500 V.

Figure 2.7.47 shows the resulting particle distribution at the entry to the RFQ. The total transverse emittance of 2.5 mm mrad is larger than the aimed design value of 1.8 mm mrad (normalized). However, this growth is mainly due to halo particles (10%) and the normalized brilliance of 40 mA/µm is still well beyond the target brilliance of 17 mA/µm as demonstrated in Fig. 2.7.48.

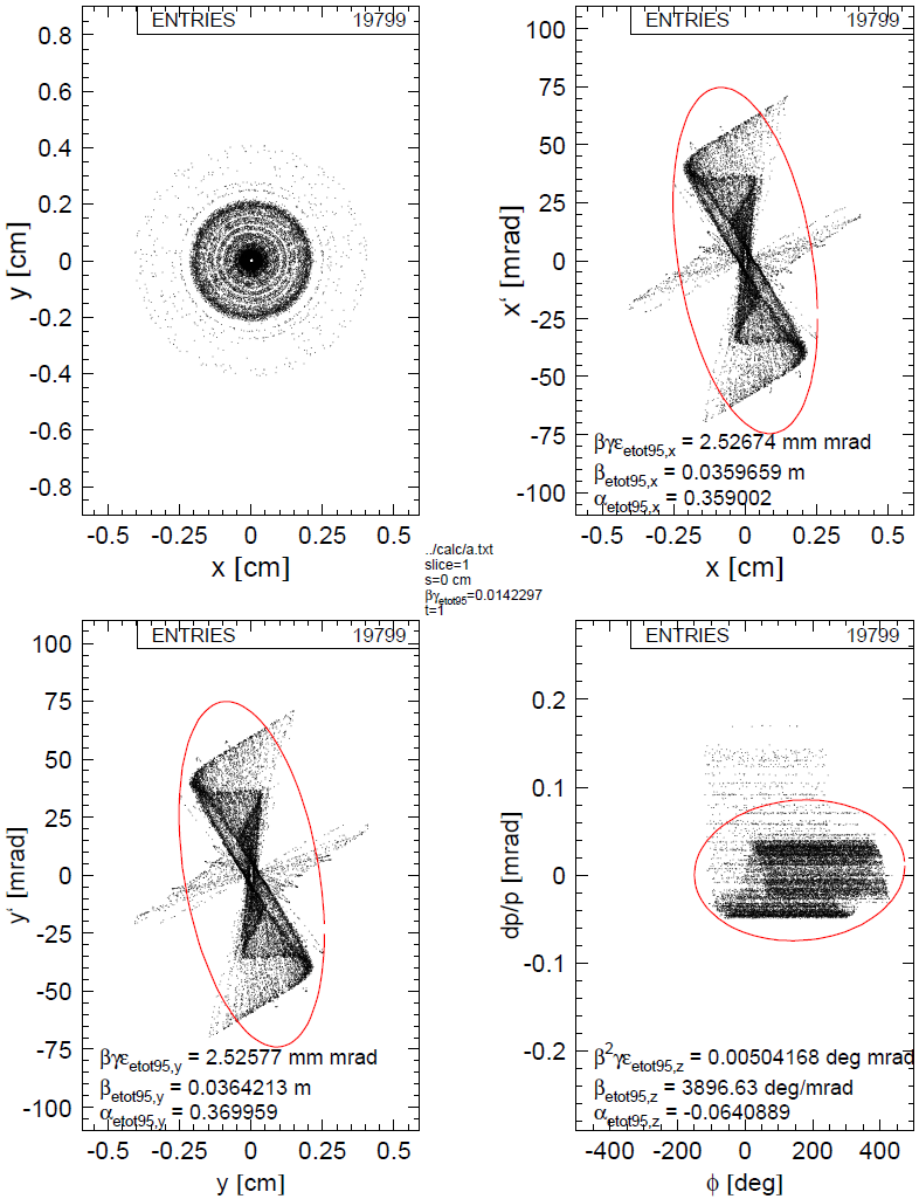

Figure 2.7.47: Phase space distribution at the entrance to the RFQ as simulated using TraceWin and SOLMAXP.

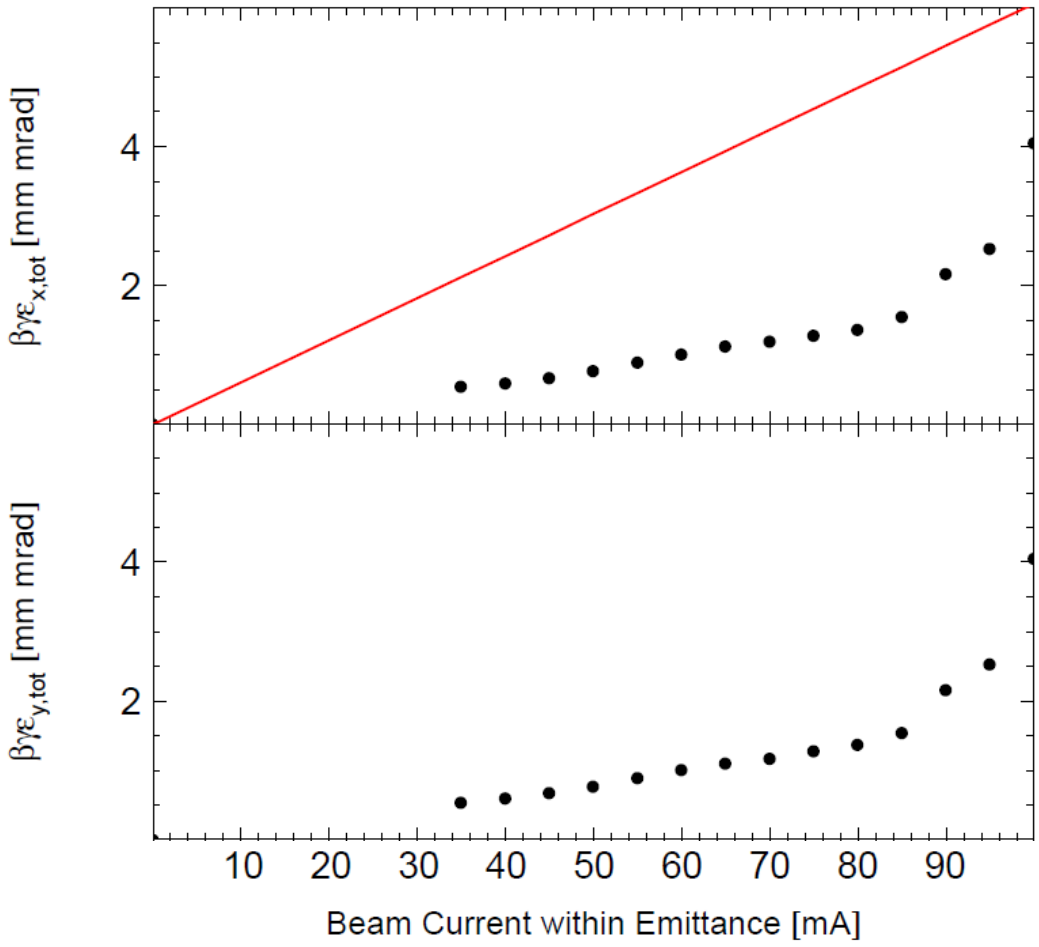

Figure 2.7.48: Normalized total emittance as function of the beam current confined by the emittance at the entrance to the RFQ. The required brilliance at the SIS18 is indicated by a red line.

2.7.11 Special Installations

2.7.11.2 Chopper

The pulse length from the LEBT has to shortened prior to injection into the RF-sections of the linac. Chopping is done right in front of the RFQ by an electrostatic device. Its conceptual design is depicted in Fig. 2.7.49. Two plates are charged to ±15 kV, respectively, when the beam needs to be chopped. Its overall length is 360 mm and its main parameters are listed in Tab. 2.7.11. A repeller electrode (black) is installed at the chopper entry and at its exit. The bias voltage is -2 kV and -1 kV, respectively. The entrance repeller is protected by a grounded electrode (red) from primary protons. Shielding of high voltage feed-throughs (not shown) from sputtered copper from the collector cone is provided by proper shaping of the cone and the deflecting plates.

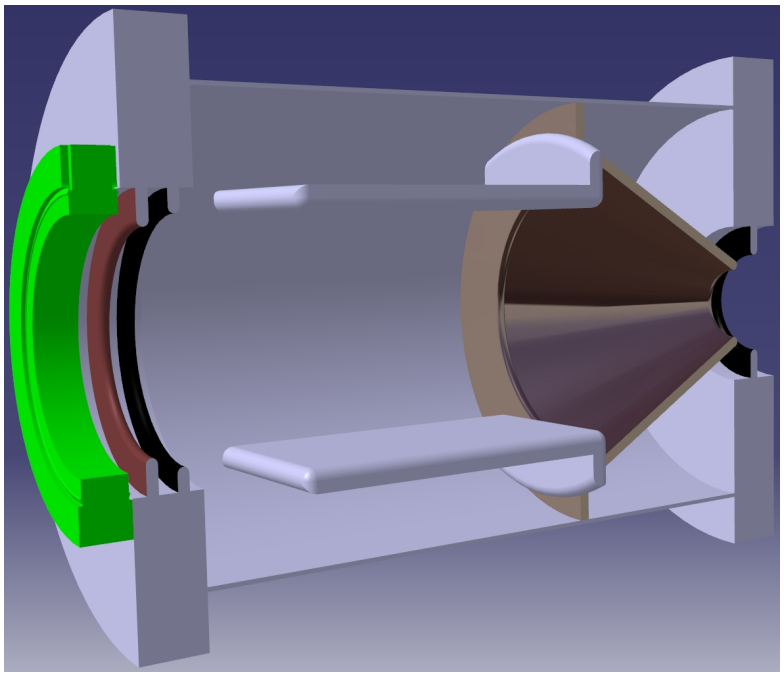

Figure 2.7.49: Conceptual layout of the chopper at the entrance to the RFQ. Its overall length is 360 mm.

Table 2.7.11: Main parameters of the chopper at the RFQ entrance.

Beam convergence angle	3.61 deg
Chopper type	electrostatic
Inter-plate voltage	30 kV (± 15 kV per plate)
Inter-plate distance	100 mm
Total capicity (incl. cables)	100 pF
Rise / fall time (e-fold)	0.25 µs, i.e.81 bunches
Chopping angle	13.3 deg
Peak intensity on cone	5.5 kW/cm^2
Total length	360 mm

Good beam length	18 – 50 μs

References

[1] Z. Li, R. Tiede, U. Ratzinger, H. Podlech, G. Clemente, K. Dermati, W. Barth, L. Groening, *Design of the R.T. CH-Cavity and Perspectives for a New GSI Proton Linac*, Proc. of the XXII Linac Conference, Lübeck, Germany, (2004).

[2] U. Ratzinger and R. Tiede, *Status of the HIIF RF Linac Study Based on H-Mode Cavities*, NIM A 415, (1998).

[3] G. Clemente, *Beam Dynamics Layout of the FAIR Proton Injector,* Proc. of the ICFA HB2008 Workshop, Nashville, U.S.A., (2008).

[4] N. Chauvin , O. Delferrière, R. Duperrier, R. Gobin, P.A.P. Nghiem, D. Uriot, M. Comunian, *Final design of the IFMIF-EVEDA low energy beam transport line*, Proc. of the 23rd Part. Accel. Conf., Vancouver, Canada, (2009).

[5] W. Vinzenz, *RF-System for the FAIR Proton Linac*, Mini-TAC Meeting at GSI, 26th of October, 2005.

[6] A. Schempp, *New Developments in High Duty Cycle, High Current RFQ's*, Proc. of the XXI Linac Conf., Gyeongju, Korea, (2002).

[7] T. Basak, B. Biswas, S. Kailas, S. Krishnagopal, Arvind Kumar, Rajni Pande, P.K. Nema, S.V.L.S. Rao, Shweta Roy, V.C. Sahni, and P. Singh, *Physics Design of a Low Energy High Intensity Proton Accelerator*, Babha Atomic Research Centre, Mumbay, India, (2004).

[8] C. Zhang and A. Schempp, *Design of an upgradeable 45–100mA RFQ accelerator for FAIR*, Nucl. Instrum & Methods in Phys. Res. **A** 609, (2009), p. 95.

[9] C. Zhang and A. Schempp, *Beam dynamics studies on a 200mA proton radio frequency quadrupole accelerator,* Nucl. Instrum & Methods in Phys. Res. **A** 586, (2008), p. 153.

[10] S. Yaramyshev et al., *Development of the versatile multi-particle code DYNAMION*, Nucl. Instrum. Methods Phys. Res., Sect. A 558, 90 (2006).

[11] http://irfu.cea.fr/Sacm/logiciels/index.php.

[12] S. Yaramyshev, W. Barth, L. Groening, Parameter study for the 325 MHz RFQ (p-Linac for FAIR), GSI internal report Dec. 2009.

[13] A. Schempp, B. Hofmann, L. Bendel, *CDR for a 352 MHz-Proton-RFQ for GSI*, Proc. of the XXII Linac Conference, Lübeck, Germany, (2004).

[14] G. Clemente, H. Podlech, R. Tiede, U. Ratzinger, L. Groening, S. Minaev, *Beam Dynamics Investigation of the first tank of a 70 mA CH-DTL Proton Injector* CH-DTL Proton Injector, CARE Note 2005-016-HIPPI.

[15] U. Ratzinger, G. Clemente, C. Commenda, H. Liebermann, H. Podlech, R. Tiede, W. Barth, L. Groening, *A 70 MeV Proton Linac for the FAIR Facility Based on CH-Cavities*, Proc. of the XIII Linac Conf. Oak Ridge, U.S.A., (2006).

[16] U. Ratzinger, G. Clemente, R. Tiede, *The RF model construction for the second accelerating module of the FAIR Proton Injector*, Report Goethe University of Frankfurt, No. 4500064849/27.07.2006

[17] R. Brodhage, U. Ratzinger, H. Podlech, G. Clemente, S. Minaev, R. Tiede, *Status of the Prototype Construction of the second cavity for the FAIR proton linac***,** Report Goethe University of Frankfurt, No. IAP-ACCC-260609.

[18] P. Strehl, *Thermal Aspects of Beam Intercepting Diagnostic Devices,* Proc. of the 5th Europ. Part. Acc. Conf., Sitges, Spain, (1996).

[19] H. Reeg and N. Schneider, *Current Transformers for GSI's keV/u to GeV/u Ion Beam - An Overview,* Proc. of the 5th DIPAC Conference, Grenoble, France, (2001).

[20] R. Gobin, P.-Y. Beauvais, K. Benmeziane, D. Bogard, G. Charruau, D. De Menezes, O. Delferrière, R. Ferdinand, A. France, Y. Gauthier, F. Harrault, J.-L. Jannin, J.-M. Lagniel, P. Mattéi, A. Sinanna, P. Ausset, S. Bousson, D. Gardes, B. Pottin, L. Celona, D. Sherman, *Saclay High Intensity Light Ion Source Status*, Proc. of the 8th Europ. Part. Acc. Conf., Paris, France, (2002).

[21] P. Ausset, S. Bousson, D. Gardès, A.C. Mueller, B. Pottin, *Optical Transverse Beam Profile Measurements for high Power Proton Beams.,* Proc. of the 8th Euro. Part. Acc. Conf., Paris, France, (2002).

[22] *The Report from the 2nd Meeting of the Technical Advisory Committee of the International Facility for Antiprotons and Ions Research*, GSI Darmstadt, Germany, December 15th, (2004).

[23] P. Forck and A. Bank, *Residual Gas Fluorescence for Profile Measurements at the GSI UNILAC*, Proc. of the 8th Europ. Part. Acc. Conf., Paris, France, (2002).

[24] F. Wolfheimer and Th. Weiland, *Untersuchung verschiedener Elektrodengeometrien für Strahlpositionsmonitore im Rahmen des FAIR Projektes der GSI*, Report Technical University of Darmstadt.

[25] P. Forck, C. Dorn, M. Herty, P. Strehl, V. Peplov, S. Sharamentov, *A Novel Device for Non-Intersecting Bunch Shape Measurement at the High Current GSI-LINAC,* Proc. of the 9th Europ. Part. Acc. Conf., Lucerne, Switzerland, (2004).

[26] R. Hollinger, W. Barth, L. Dahl, M. Galonska, L. Groening, R. Gobin, O. Meusel, P. A. Leroy, P. Spaedtke, *High-Current Proton beam Investigations at the SILHI-LEBT at CEA/Saclay*, Proc. of the XXIII Linac Conference, Knoxville, USA, (2006).

[27] R. Gobin, V. Blideanu, D. Bogard, G. Bourdelle, N. Chauvin, O. Delferrière, P. Girardot, J.L. Jannin, S. Langlois, D. Loiseau, B. Pottin, J-Y. Rousse, F. Senée, *General design of the*

IFMIF deuteron injector: source and beam line, Proc. of the 13th ICIS Conf., Gatlinburg, U.S.A., (2009).